

## *Fermi* Large Area Telescope Constraints on the Gamma-ray Opacity of the Universe

A. A. Abdo<sup>1,2</sup>, M. Ackermann<sup>3</sup>, M. Ajello<sup>3</sup>, A. Allafort<sup>3</sup>, W. B. Atwood<sup>4</sup>, L. Baldini<sup>5</sup>,  
 J. Ballet<sup>6</sup>, G. Barbiellini<sup>7,8</sup>, M. G. Baring<sup>9</sup>, D. Bastieri<sup>10,11</sup>, B. M. Baughman<sup>12</sup>,  
 K. Bechtol<sup>3</sup>, R. Bellazzini<sup>5</sup>, B. Berenji<sup>3</sup>, P. N. Bhat<sup>13</sup>, R. D. Blandford<sup>3</sup>, E. D. Bloom<sup>3</sup>,  
 E. Bonamente<sup>14,15</sup>, A. W. Borgland<sup>3</sup>, A. Bouvier<sup>0,3</sup>, T. J. Brandt<sup>16,12</sup>, J. Bregeon<sup>5</sup>,  
 A. Brez<sup>5</sup>, M. S. Briggs<sup>13</sup>, M. Brigida<sup>17,18</sup>, P. Bruel<sup>19</sup>, R. Buehler<sup>3</sup>, T. H. Burnett<sup>20</sup>,  
 S. Buson<sup>10,11</sup>, G. A. Caliendo<sup>21</sup>, R. A. Cameron<sup>3</sup>, P. A. Caraveo<sup>22</sup>, S. Carrigan<sup>11</sup>,  
 J. M. Casandjian<sup>6</sup>, E. Cavazzuti<sup>23</sup>, C. Cecchi<sup>14,15</sup>, Ö. Çelik<sup>24,25,26</sup>, E. Charles<sup>3</sup>,  
 A. Chekhtman<sup>1,27</sup>, A. W. Chen<sup>0,22</sup>, C. C. Cheung<sup>1,2</sup>, J. Chiang<sup>3</sup>, S. Ciprini<sup>15</sup>, R. Claus<sup>3</sup>,  
 J. Cohen-Tanugi<sup>28</sup>, V. Connaughton<sup>13</sup>, J. Conrad<sup>29,30,31</sup>, L. Costamante<sup>3</sup>, C. D. Dermer<sup>1</sup>,  
 A. de Angelis<sup>32</sup>, F. de Palma<sup>17,18</sup>, S. W. Digel<sup>3</sup>, B. L. Dingus<sup>33</sup>, E. do Couto e Silva<sup>3</sup>,  
 P. S. Drell<sup>3</sup>, R. Dubois<sup>3</sup>, C. Favuzzi<sup>17,18</sup>, S. J. Fegan<sup>19</sup>, J. Finke<sup>1,2</sup>, P. Fortin<sup>19</sup>,  
 Y. Fukazawa<sup>34</sup>, S. Funk<sup>3</sup>, P. Fusco<sup>17,18</sup>, F. Gargano<sup>18</sup>, D. Gasparri<sup>23</sup>, N. Gehrels<sup>24</sup>,  
 S. Germani<sup>14,15</sup>, N. Giglietto<sup>17,18</sup>, R. C. Gilmore<sup>4</sup>, P. Giommi<sup>23</sup>, F. Giordano<sup>17,18</sup>,  
 M. Giroletti<sup>35</sup>, T. Glanzman<sup>3</sup>, G. Godfrey<sup>3</sup>, J. Granot<sup>36</sup>, J. Greiner<sup>37</sup>, I. A. Grenier<sup>6</sup>,  
 J. E. Grove<sup>1</sup>, S. Guiriec<sup>13</sup>, M. Gustafsson<sup>10</sup>, D. Hadasch<sup>38</sup>, M. Hayashida<sup>3</sup>, E. Hays<sup>24</sup>,  
 D. Horan<sup>19</sup>, R. E. Hughes<sup>12</sup>, G. Jóhannesson<sup>3</sup>, A. S. Johnson<sup>3</sup>, R. P. Johnson<sup>4</sup>,  
 W. N. Johnson<sup>1</sup>, T. Kamae<sup>3</sup>, H. Katagiri<sup>34</sup>, J. Kataoka<sup>39</sup>, J. Knödseder<sup>16</sup>, D. Kocevski<sup>3</sup>,  
 M. Kuss<sup>5</sup>, J. Lande<sup>3</sup>, L. Latronico<sup>5</sup>, S.-H. Lee<sup>3</sup>, M. Llena Garde<sup>29,30</sup>, F. Longo<sup>7,8</sup>,  
 F. Loparco<sup>17,18</sup>, B. Lott<sup>40,41</sup>, M. N. Lovellette<sup>1</sup>, P. Lubrano<sup>14,15</sup>, A. Makeev<sup>1,27</sup>,  
 M. N. Mazziotta<sup>18</sup>, W. McConville<sup>24,42</sup>, J. E. McEnery<sup>24,42</sup>, S. McGlynn<sup>43,30</sup>, J. Mehault<sup>28</sup>,  
 P. Mészáros<sup>44</sup>, P. F. Michelson<sup>3</sup>, T. Mizuno<sup>34</sup>, A. A. Moiseev<sup>25,42</sup>, C. Monte<sup>17,18</sup>,  
 M. E. Monzani<sup>3</sup>, E. Moretti<sup>7,8</sup>, A. Morselli<sup>45</sup>, I. V. Moskalenko<sup>3</sup>, S. Murgia<sup>3</sup>,  
 T. Nakamori<sup>39</sup>, M. Naumann-Godo<sup>6</sup>, P. L. Nolan<sup>3</sup>, J. P. Norris<sup>46</sup>, E. Nuss<sup>28</sup>, M. Ohno<sup>47</sup>,  
 T. Ohsugi<sup>48</sup>, A. Okumura<sup>47</sup>, N. Omodei<sup>3</sup>, E. Orlando<sup>37</sup>, J. F. Ormes<sup>46</sup>, M. Ozaki<sup>47</sup>,  
 D. Paneque<sup>3</sup>, J. H. Panetta<sup>3</sup>, D. Parent<sup>1,27</sup>, V. Pelassa<sup>28</sup>, M. Pepe<sup>14,15</sup>, M. Pesce-Rollins<sup>5</sup>,  
 F. Piron<sup>28</sup>, T. A. Porter<sup>3</sup>, J. R. Primack<sup>4</sup>, S. Rainò<sup>0,17,18</sup>, R. Rando<sup>10,11</sup>, M. Razzano<sup>5</sup>,  
 S. Razzaque<sup>0,1,2</sup>, A. Reimer<sup>0,49,3</sup>, O. Reimer<sup>49,3</sup>, L. C. Reyes<sup>0,50</sup>, J. Ripken<sup>29,30</sup>, S. Ritz<sup>4</sup>,  
 R. W. Romani<sup>3</sup>, M. Roth<sup>20</sup>, H. F.-W. Sadrozinski<sup>4</sup>, D. Sanchez<sup>19</sup>, A. Sander<sup>12</sup>,  
 J. D. Scargle<sup>51</sup>, T. L. Schalk<sup>4</sup>, C. Sgrò<sup>5</sup>, M. S. Shaw<sup>3</sup>, E. J. Siskind<sup>52</sup>, P. D. Smith<sup>12</sup>,  
 G. Spandre<sup>5</sup>, P. Spinelli<sup>17,18</sup>, F. W. Stecker<sup>24</sup>, M. S. Strickman<sup>1</sup>, D. J. Suson<sup>53</sup>, H. Tajima<sup>3</sup>,  
 H. Takahashi<sup>48</sup>, T. Takahashi<sup>47</sup>, T. Tanaka<sup>3</sup>, J. B. Thayer<sup>3</sup>, J. G. Thayer<sup>3</sup>,  
 D. J. Thompson<sup>24</sup>, L. Tibaldo<sup>10,11,6,54</sup>, D. F. Torres<sup>21,38</sup>, G. Tosti<sup>14,15</sup>, A. Tramacere<sup>3,55,56</sup>,  
 Y. Uchiyama<sup>3</sup>, T. L. Usher<sup>3</sup>, J. Vandenbroucke<sup>3</sup>, V. Vasileiou<sup>25,26</sup>, N. Vilchez<sup>16</sup>,

<sup>36</sup> V. Vitale<sup>45,57</sup>, A. von Kienlin<sup>37</sup>, A. P. Waite<sup>3</sup>, P. Wang<sup>3</sup>, C. Wilson-Hodge<sup>58</sup>, B. L. Winer<sup>12</sup>,  
<sup>37</sup> K. S. Wood<sup>1</sup>, R. Yamazaki<sup>59</sup>, Z. Yang<sup>29,30</sup>, T. Ylinen<sup>43,60,30</sup>, M. Ziegler<sup>4</sup>

---

<sup>0</sup>**Corresponding authors:** A. Bouvier, bouvier@stanford.edu; A. Chen, chen@iasf-milano.inaf.it; S. Raino, silvia.raino@ba.infn.it; S. Razzaque, md.razzaque.ctr.bg@nrl.navy.mil, A. Reimer, anita.reimer@uibk.ac.at; L. C. Reyes, lreyes@kip.uchicago.edu

<sup>1</sup>Space Science Division, Naval Research Laboratory, Washington, DC 20375, USA

<sup>2</sup>National Research Council Research Associate, National Academy of Sciences, Washington, DC 20001, USA

<sup>3</sup>W. W. Hansen Experimental Physics Laboratory, Kavli Institute for Particle Astrophysics and Cosmology, Department of Physics and SLAC National Accelerator Laboratory, Stanford University, Stanford, CA 94305, USA

<sup>4</sup>Santa Cruz Institute for Particle Physics, Department of Physics and Department of Astronomy and Astrophysics, University of California at Santa Cruz, Santa Cruz, CA 95064, USA

<sup>5</sup>Istituto Nazionale di Fisica Nucleare, Sezione di Pisa, I-56127 Pisa, Italy

<sup>6</sup>Laboratoire AIM, CEA-IRFU/CNRS/Université Paris Diderot, Service d’Astrophysique, CEA Saclay, 91191 Gif sur Yvette, France

<sup>7</sup>Istituto Nazionale di Fisica Nucleare, Sezione di Trieste, I-34127 Trieste, Italy

<sup>8</sup>Dipartimento di Fisica, Università di Trieste, I-34127 Trieste, Italy

<sup>9</sup>Rice University, Department of Physics and Astronomy, MS-108, P. O. Box 1892, Houston, TX 77251, USA

<sup>10</sup>Istituto Nazionale di Fisica Nucleare, Sezione di Padova, I-35131 Padova, Italy

<sup>11</sup>Dipartimento di Fisica “G. Galilei”, Università di Padova, I-35131 Padova, Italy

<sup>12</sup>Department of Physics, Center for Cosmology and Astro-Particle Physics, The Ohio State University, Columbus, OH 43210, USA

<sup>13</sup>Center for Space Plasma and Aeronomic Research (CSPAR), University of Alabama in Huntsville, Huntsville, AL 35899, USA

<sup>14</sup>Istituto Nazionale di Fisica Nucleare, Sezione di Perugia, I-06123 Perugia, Italy

<sup>15</sup>Dipartimento di Fisica, Università degli Studi di Perugia, I-06123 Perugia, Italy

<sup>16</sup>Centre d’Étude Spatiale des Rayonnements, CNRS/UPS, BP 44346, F-30128 Toulouse Cedex 4, France

<sup>17</sup>Dipartimento di Fisica “M. Merlin” dell’Università e del Politecnico di Bari, I-70126 Bari, Italy

<sup>18</sup>Istituto Nazionale di Fisica Nucleare, Sezione di Bari, 70126 Bari, Italy

<sup>19</sup>Laboratoire Leprince-Ringuet, École polytechnique, CNRS/IN2P3, Palaiseau, France

<sup>20</sup>Department of Physics, University of Washington, Seattle, WA 98195-1560, USA

<sup>21</sup>Institut de Ciències de l’Espai (IEEC-CSIC), Campus UAB, 08193 Barcelona, Spain

<sup>22</sup>INAF-Istituto di Astrofisica Spaziale e Fisica Cosmica, I-20133 Milano, Italy

- 
- <sup>23</sup>Agenzia Spaziale Italiana (ASI) Science Data Center, I-00044 Frascati (Roma), Italy
- <sup>24</sup>NASA Goddard Space Flight Center, Greenbelt, MD 20771, USA
- <sup>25</sup>Center for Research and Exploration in Space Science and Technology (CRESST) and NASA Goddard Space Flight Center, Greenbelt, MD 20771, USA
- <sup>26</sup>Department of Physics and Center for Space Sciences and Technology, University of Maryland Baltimore County, Baltimore, MD 21250, USA
- <sup>27</sup>George Mason University, Fairfax, VA 22030, USA
- <sup>28</sup>Laboratoire de Physique Théorique et Astroparticules, Université Montpellier 2, CNRS/IN2P3, Montpellier, France
- <sup>29</sup>Department of Physics, Stockholm University, AlbaNova, SE-106 91 Stockholm, Sweden
- <sup>30</sup>The Oskar Klein Centre for Cosmoparticle Physics, AlbaNova, SE-106 91 Stockholm, Sweden
- <sup>31</sup>Royal Swedish Academy of Sciences Research Fellow, funded by a grant from the K. A. Wallenberg Foundation
- <sup>32</sup>Dipartimento di Fisica, Università di Udine and Istituto Nazionale di Fisica Nucleare, Sezione di Trieste, Gruppo Collegato di Udine, I-33100 Udine, Italy
- <sup>33</sup>Los Alamos National Laboratory, Los Alamos, NM 87545, USA
- <sup>34</sup>Department of Physical Sciences, Hiroshima University, Higashi-Hiroshima, Hiroshima 739-8526, Japan
- <sup>35</sup>INAF Istituto di Radioastronomia, 40129 Bologna, Italy
- <sup>36</sup>Centre for Astrophysics Research, Science and Technology Research Institute, University of Hertfordshire, Hatfield AL10 9AB, UK
- <sup>37</sup>Max-Planck Institut für extraterrestrische Physik, 85748 Garching, Germany
- <sup>38</sup>Institució Catalana de Recerca i Estudis Avançats (ICREA), Barcelona, Spain
- <sup>39</sup>Research Institute for Science and Engineering, Waseda University, 3-4-1, Okubo, Shinjuku, Tokyo, 169-8555 Japan
- <sup>40</sup>CNRS/IN2P3, Centre d'Études Nucléaires Bordeaux Gradignan, UMR 5797, Gradignan, 33175, France
- <sup>41</sup>Université de Bordeaux, Centre d'Études Nucléaires Bordeaux Gradignan, UMR 5797, Gradignan, 33175, France
- <sup>42</sup>Department of Physics and Department of Astronomy, University of Maryland, College Park, MD 20742, USA
- <sup>43</sup>Department of Physics, Royal Institute of Technology (KTH), AlbaNova, SE-106 91 Stockholm, Sweden
- <sup>44</sup>Department of Astronomy and Astrophysics, Pennsylvania State University, University Park, PA 16802, USA
- <sup>45</sup>Istituto Nazionale di Fisica Nucleare, Sezione di Roma “Tor Vergata”, I-00133 Roma, Italy

## ABSTRACT

38

39

The Extragalactic Background Light (EBL) includes photons with wavelengths from ultraviolet to infrared, which are effective at attenuating gamma rays with energy above  $\sim 10$  GeV during propagation from sources at cosmological distances. This results in a redshift- and energy-dependent attenuation of the  $\gamma$ -ray flux of extragalactic sources such as blazars and Gamma-Ray Bursts (GRBs). The Large Area Telescope onboard *Fermi* detects a sample of  $\gamma$ -ray blazars with redshift up to  $z \sim 3$ , and GRBs with redshift up to  $z \sim 4.3$ . Using photons above 10 GeV collected by *Fermi* over more than one year of observations for these sources, we investigate the effects of the EBL on the  $\gamma$ -ray flux. We constrain the  $\gamma$ -ray opacity of the Universe at various energies and redshifts, and compare this with predictions from well-known EBL models. We find that an EBL intensity in the optical–ultraviolet wavelengths as great as predicted by the “fast-evolution” and “baseline” models of Stecker et al. (2006) can be ruled out with high confidence.

---

<sup>46</sup>Department of Physics and Astronomy, University of Denver, Denver, CO 80208, USA

<sup>47</sup>Institute of Space and Astronautical Science, JAXA, 3-1-1 Yoshinodai, Sagami-hara, Kanagawa 229-8510, Japan

<sup>48</sup>Hiroshima Astrophysical Science Center, Hiroshima University, Higashi-Hiroshima, Hiroshima 739-8526, Japan

<sup>49</sup>Institut für Astro- und Teilchenphysik and Institut für Theoretische Physik, Leopold-Franzens-Universität Innsbruck, A-6020 Innsbruck, Austria

<sup>50</sup>Kavli Institute for Cosmological Physics, University of Chicago, Chicago, IL 60637, USA

<sup>51</sup>Space Sciences Division, NASA Ames Research Center, Moffett Field, CA 94035-1000, USA

<sup>52</sup>NYCB Real-Time Computing Inc., Lattingtown, NY 11560-1025, USA

<sup>53</sup>Department of Chemistry and Physics, Purdue University Calumet, Hammond, IN 46323-2094, USA

<sup>54</sup>Partially supported by the International Doctorate on Astroparticle Physics (IDAPP) program

<sup>55</sup>Consorzio Interuniversitario per la Fisica Spaziale (CIFS), I-10133 Torino, Italy

<sup>56</sup>INTEGRAL Science Data Centre, CH-1290 Versoix, Switzerland

<sup>57</sup>Dipartimento di Fisica, Università di Roma “Tor Vergata”, I-00133 Roma, Italy

<sup>58</sup>NASA Marshall Space Flight Center, Huntsville, AL 35812, USA

<sup>59</sup>Aoyama Gakuin University, Sagami-hara-shi, Kanagawa 229-8558, Japan

<sup>60</sup>School of Pure and Applied Natural Sciences, University of Kalmar, SE-391 82 Kalmar, Sweden

40 *Subject headings:* diffuse radiation – dust, extinction – gamma rays: observations

41 **1. Introduction**

42 The *Fermi* Gamma Ray Space Telescope was launched on 2008 June 11<sup>th</sup> to provide  
 43 an unprecedented view of the  $\gamma$ -ray Universe. The main instrument onboard *Fermi*, the  
 44 Large Area Telescope (LAT), offers a broader bandpass ( $\sim 20$  MeV to over 300 GeV;  
 45 Atwood et al. 2009) and improved sensitivity (by greater than an order of magnitude) than  
 46 that of its predecessor instrument EGRET onboard the *Compton Gamma Ray Observa-*  
 47 *tory* (Thompson et al. 1993), and the Italian Space Agency satellite *AGILE* (Tavani et al.  
 48 2008), which was launched in 2007. The LAT observes the full sky every 3 hr in survey  
 49 mode leading to a broadly uniform exposure with less than  $\sim 15\%$  variation. The Gamma-  
 50 ray Burst Monitor, the lower energy ( $\sim 8$  keV – 40 MeV) instrument onboard *Fermi*, observes  
 51 the full un-occulted sky at all times and provides alerts for transient sources such as GRBs.

52 A major science goal of *Fermi* is to probe the opacity of the Universe to high-energy (HE)  
 53  $\gamma$ -rays as they propagate from their sources to Earth. Such energetic photons are subject to  
 54 absorption by production of electron-positron ( $e^-e^+$ ) pairs while interacting with low energy  
 55 cosmic background photons (Nishikov 1961; Gould & Shröder 1966; Fazio & Stecker 1970)  
 56 if above the interaction threshold:  $\epsilon_{\text{thr}} = (2m_e c^2)^2 / (2E(1 - \mu))$  where  $\epsilon$  and  $E$  denote the  
 57 energies of the background photon and  $\gamma$  ray, respectively, in the comoving frame of the  
 58 interaction,  $m_e c^2$  is the rest mass electron energy, and  $\theta = \arccos(\mu)$  the interaction angle.  
 59 Because of the sharply peaked cross section close to threshold, most interactions are centered  
 60 around  $\epsilon^* \approx 0.8(E/\text{TeV})^{-1}\text{eV}$  for a smooth broadband spectrum. Thus, the extragalactic  
 61 background light (EBL) at UV through optical wavelengths constitutes the main source of  
 62 opacity for  $\gamma$ -rays from extragalactic sources (Active Galactic Nuclei: AGN and GRBs) in  
 63 the LAT energy range. The effect of absorption of HE  $\gamma$ -rays is then reflected in an energy-  
 64 and redshift dependent softening of the observed spectrum from a distant  $\gamma$ -ray source. The  
 65 observation, or absence, of such spectral features at HEs, for a source at redshift  $z$  can be  
 66 used to constrain the  $\gamma\gamma \rightarrow e^+e^-$  pair production opacity,  $\tau_{\gamma\gamma}(E, z)$ .

67 The EBL is the accumulated radiation from structure formation and its cosmological  
 68 evolution. Knowledge of its intensity variation with time would probe models of galaxy  
 69 and star formation. The intensity of the EBL from the near-IR to ultraviolet is thought to  
 70 be dominated by direct starlight emission out to large redshifts, and to a lesser extent by  
 71 optically bright AGN. At longer wavelengths the infrared background is produced by thermal

72 radiation from dust which is heated by starlight, and also emission from polycyclic aromatic  
73 hydrocarbons (see e.g. Driver et al. 2008).

74 Direct measurements of the EBL is difficult due to contamination by foreground zodiacal  
75 and Galactic light (e.g., Hauser & Dwek 2001), and galaxy counts result in a lower limit since  
76 the number of unresolved sources is unknown (e.g., Madau & Pozzetti 2000). A number  
77 of EBL models have been developed over the last two decades (e.g., Salamon & Stecker  
78 1998; Stecker et al. 2006; Kneiske et al. 2002, 2004; Primack et al. 2005; Gilmore et al. 2009;  
79 Franceschini et al. 2008; Razzaque et al. 2009; Finke et al. 2010), however large scatter in  
80 available EBL data does not constrain these models strongly.

81 The primary extragalactic  $\gamma$ -ray sources are blazars, which are galaxies with relativistic  
82 jets directed along our line of sight; and GRBs, where at least some long ( $> 2$  s) GRBs  
83 are associated with core collapse of supernovae of type Ic and therefore with the collapse  
84 of a massive star, while short ( $< 2$  s) GRBs might be caused by binary mergers of neutron  
85 stars or neutron star - black hole systems. Both types of GRBs produce beamed high-energy  
86 radiation during an intense prompt emission phase. GRBs have not been used to constrain  
87 EBL absorption during the pre-*Fermi* era mainly because of a lack of sensitivity to transient  
88 objects above 10 GeV.

89 The sensitivity of EGRET decreased significantly above 10 GeV, and the field-of-view  
90 (FoV) of TeV instruments is too small to catch the prompt phase where most of the HE  
91 emission occurs. The new energy window (10 – 300 GeV) accessible by *Fermi*, and the wide  
92 FoV of the LAT, makes GRBs interesting targets to constrain EBL absorption in this energy  
93 band.

94 Evaluating the ratio of the putatively absorbed to unabsorbed fluxes from a large number  
95 of distant blazars and GRBs observed by *Fermi* could result in interesting EBL constraints,  
96 as proposed by Chen et al. (2004), although intrinsic spectral curvature (e.g., Massaro et al.  
97 2006) or  $z$ -dependent source internal absorption (Reimer 2007) could make this, or similar  
98 techniques, less effective. Georganopoulos et al. (2008) have proposed that Compton scat-  
99 tering of the EBL by the radio lobes of nearby radio galaxies such as Fornax A could be  
100 detectable by the *Fermi*-LAT. If identified as unambiguously originating from such process,  
101 a LAT detection of Fornax A could constrain the local EBL intensity.

102 Because the e-folding cutoff energy,  $E(\tau_{\gamma\gamma} = 1)$ , from  $\gamma\gamma$  pair production in  $\gamma$ -ray  
103 source spectra decreases with redshift, TeV  $\gamma$ -ray telescopes are limited to probing EBL  
104 absorption at low redshift (e.g.,  $\lesssim 0.5$ ) due to their high detection thresholds typically at  
105 100 GeV to 300 GeV. Ground-based  $\gamma$ -ray telescopes have detected 35 extragalactic sources

106 to date<sup>1</sup>, mostly of the high-synchrotron peaked (HSP) BL Lacertae objects type. The most  
 107 distant sources seen from the ground with a confirmed redshift are the flat spectrum radio  
 108 quasar (FSRQ) 3C 279 at  $z = 0.536$  (Albert et al. 2008) and PKS 1510-089 at  $z = 0.36$   
 109 (Wagner et al. 2010). Observations of the closest sources at multi-TeV energies have been  
 110 effective in placing limits on the local EBL at mid-IR wavelengths, while spectra of more  
 111 distant sources generally do not extend above 1 TeV, and therefore probe the optical and  
 112 near-IR starlight peak of the intervening EBL.

113 The starting point for constraining the EBL intensity from observation of TeV  $\gamma$ -rays  
 114 from distant blazars with atmospheric Cherenkov telescopes (e.g., Stecker & de Jager 1993;  
 115 Stanev & Franceschini 1998; Schroedter 2005; Aharonian et al. 1999, 2002; Costamante et al.  
 116 2004; Aharonian et al. 2006; Mazin & Raue 2007; Albert et al. 2008; Krennrich et al. 2008;  
 117 Finke & Razzaque 2009) is the assumption of a reasonable intrinsic blazar spectrum, which,  
 118 in the case of a power law,  $dN/dE \propto E^{-\Gamma_{int}}$  for example, that is not harder than a pre-  
 119 specified minimum value, e.g.,  $\Gamma_{int} \geq \Gamma_{min} = 0.67$  or 1.5. Upper limits on the EBL intensity  
 120 are obtained when the reconstructed intrinsic spectral index from the observed spectrum,  
 121  $\Gamma_{obs}$ , presumably softened by EBL absorption of very high energy (VHE)  $\gamma$ -rays, is required  
 122 to not fall below  $\Gamma_{int}$ . The minimum value of  $\Gamma$  has been a matter of much debate, being  
 123 reasoned to be  $\Gamma_{int} = 1.5$  by Aharonian et al. (2006) from simple shock acceleration the-  
 124 ory and from the observed spectral energy distribution (SED) properties of blazars, while  
 125 Stecker et al. (2007) argued for harder values under specific conditions based based on more  
 126 detailed shock acceleration simulations. Katarzyński et al. (2006) suggested that a spectral  
 127 index as hard as  $\Gamma_{int} = 0.67$  was possible in a single-zone leptonic model if the underly-  
 128 ing electron spectrum responsible for inverse-Compton emission had a sharp lower-energy  
 129 cutoff. Böttcher et al. (2008) noted that Compton scattering of the cosmic microwave back-  
 130 ground radiation by extended jets could lead to harder observed VHE  $\gamma$ -ray spectra, and  
 131 Aharonian et al. (2008) have argued that internal absorption could, in some cases, lead to  
 132 harder spectra in the TeV range as well.

133 A more observational approach uses the (unabsorbed) photon index as measured in  
 134 the sub-GeV range as the intrinsic spectral slope at GeV-TeV energies. This method has  
 135 recently been applied to PG 1553+113 (Abdo et al. 2010a) and 1ES 1424+240 (Acciari et al.  
 136 2010; Prandini et al. 2010) to derive upper limits on their uncertain redshifts, and to search  
 137 for EBL-induced spectral softening in *Fermi* observations of a sample of TeV-selected AGN  
 138 (Abdo et al. 2010j). There is hope that attenuation in the spectra of higher redshift objects  
 139 ( $z \gtrsim 1$ ) may be detectable at the lower energies that are accessible to the *Fermi*-LAT, i.e.,

---

<sup>1</sup>e.g., <http://www.mpi-hd.mpg.de/hfm/HESS/pages/home/sources/>, <http://www.mppmu.mpg.de/rwagner/sources/>

140 at  $E \approx 10 - 300$  GeV. Gamma rays at these energies are attenuated mainly by the evolving  
 141 UV background, which is produced primarily by young stellar populations and closely traces  
 142 the global star-formation rate. Observations with *Fermi* of sources out to high redshift could  
 143 therefore reveal information about the star-formation history of the Universe, as well as the  
 144 uncertain attenuation of UV starlight by dust.

145 In this paper we present constraints from *Fermi* blazars and GRBs on the EBL intensity  
 146 of the Universe. The highest-energy  $\gamma$ -rays from high redshift sources are the most effective  
 147 probe of the EBL intensity, and consequently a powerful tool for investigating possible sig-  
 148 natures of EBL absorption. In contrast to ground-based  $\gamma$ -ray detectors, *Fermi* offers the  
 149 possibility of probing the EBL at high redshifts by the detection of AGN at  $\gtrsim 10$  GeV ener-  
 150 gies out to  $z > 3$ , and additionally by the detection of GRB 080916C at a redshift of  $\sim 4.35$   
 151 (Abdo et al. 2009a; Greiner et al. 2009). GRBs are known to exist at even higher redshifts  
 152 (Tanvir et al. 2009, GRB 090423 is the current record holder with  $z \sim 8.2$ ). Therefore obser-  
 153 vations of these sources with *Fermi* are promising candidates for probing the optical-UV EBL  
 154 at high redshifts that are not currently accessible to ground-based (Cherenkov) telescopes.

155 In Section 2 we describe our data selections, the *Fermi* LAT AGN and GRB observations  
 156 during the first year of operation and analysis, and we discuss potential biases in the selection.  
 157 Our methodology and results are presented in Section 3. We discuss implications of our  
 158 results in Section 4, and conclude in Section 5.

159 In the following, energies are in the observer frame except where noted otherwise.

## 160 2. Observations and Data Selection

161 The *Fermi* LAT is a pair-conversion detector sensitive to  $\gamma$ -rays with energies greater  
 162 than 20 MeV. The LAT has a peak effective area  $\geq 8000$  cm<sup>2</sup> at energies greater than 1 GeV  
 163 relevant for most of the event selections considered in this analysis and a large,  $\sim 2.4$  sr,  
 164 field-of-view at any given instant. The angular resolution for the 68% containment radius is  
 165  $\sim 0.6^\circ$  for 1 GeV photons that convert in the upper layers of the tracker (front events) and  
 166 about a factor of 2 larger for those that convert in the bottom layers of the tracker (back  
 167 events). A simple acceptance-averaged approximation for the 68% containment angle that is  
 168 helpful to illustrate the energy dependent PSF is  $\langle \theta_{68}(E) \rangle = (0.8^\circ) \times (E/\text{GeV})^{-0.8} \oplus (0.07^\circ)$ .  
 169 A full description of the LAT instrument is reported in Atwood et al. (2009).

170 Our data set includes LAT events with energy above 100 MeV that were collected  
 171 between 2008 August 4<sup>th</sup> and 2009 July 4<sup>th</sup> for AGN observations. LAT-detected GRBs are  
 172 considered up to 2009 September 30<sup>th</sup>. A zenith angle cut of  $105^\circ$  was applied in order to

173 greatly reduce any contamination from the Earth albedo. Blazars and GRBs have different  
 174 emission characteristics, which result in different analysis procedures here. The event rate  
 175 detected by the LAT in the vicinity (68% confidence radius) of a blazar is largely background  
 176 dominated and only continuous observations over long time scales allow the detection of the  
 177 underlying blazar emission. To minimize the background contamination when analyzing  
 178 blazar data we use the “diffuse” class events, which provide the purest  $\gamma$ -ray sample and the  
 179 best angular resolution. GRBs, on the other hand, emit on a very short time scale where the  
 180 event rate can be considered mostly background free (at least during the prompt emission  
 181 of bright bursts). It is therefore possible to loosen the event class selection to increase the  
 182 effective area at the expense of a higher background rate which is still small on short time  
 183 scales for bright bursts. The “transient” class was designed for this specific purpose and we  
 184 use these events for GRB analysis.<sup>2</sup>

## 185 2.1. AGN sample and potential biases

186 We use high redshift blazars extracted from the First LAT AGN Catalog (1LAC;  
 187 Abdo et al. 2010e) as the AGN source sample to probe the UV through optical EBL. This  
 188 catalog contains 671 sources at high Galactic latitude ( $|b| > 10^\circ$ ) associated with high-  
 189 confidence with blazars and other AGNs that were detected with a Test Statistic<sup>3</sup> (TS)  
 190  $TS > 25$  during the first 11 months of science operation of the LAT. Detection of correlated  
 191 multiwavelength variability was required in order to establish a source as being identified.

192 Source associations were made with a Bayesian approach (similar to Mattox et al. 2001).  
 193 The Bayesian approach for source association implemented in the *gtsrcid* tool of the LAT *Sci-*  
 194 *enceTools* package<sup>4</sup> uses only spatial coincidences between LAT and the counterpart sources.  
 195 Candidate source catalogs used for this procedure include CRATES (Healey et al. 2007),  
 196 CGRaBS (Healey et al. 2008) and the Roma-BZCAT (Massaro et al. 2009), which also pro-  
 197 vide optical classifications and the latter two provide also spectroscopic redshifts for the  
 198 sources. See Abdo et al. (2010e) for further details on the source detection and association  
 199 algorithms referred to here.

200 As discussed below, some methods applied here require one to distinguish among the

---

<sup>2</sup>see Atwood et al. (2009) for further details on LAT event selection.

<sup>3</sup>The test statistic (TS) is defined as  $TS = -2 \times (\log(L_0) - \log(L_1))$  with  $L_0$  the likelihood of the Null-hypothesis model as compared to the likelihood of a competitive model,  $L_1$ , (see Section 3.2.2).

<sup>4</sup><http://fermi.gsfc.nasa.gov/ssc/data/analysis/scitools/overview.html>

201 different blazar source classes. Flat-spectrum radio quasars (FSRQs) and BL Lacs are dis-  
 202 cerned by their observed optical emission line equivalent widths and the Ca II break ratio  
 203 (e.g., Stocke et al. 1991; Marcha et al. 1996) following the procedure outlined in Abdo et al.  
 204 (2009b). The BL Lac class itself is sub-divided into Low-, Intermediate-, and High-Synchrotron  
 205 peaked BL Lacs (denoted as LSP-BLs, ISP-BLs and HSP-BLs, respectively) by estimating  
 206 the position of their synchrotron peak,  $\nu_{\text{peak}}^s$ , from the indices  $\alpha_{ox} \simeq 0.384 \cdot \log(f_{5000\text{\AA}}/f_{1\text{keV}})$   
 207 and  $\alpha_{ro} \simeq 0.197 \cdot \log(f_{5\text{GHz}}/f_{5000\text{\AA}})$  determined by the (rest frame) optical ( $f_{5000\text{\AA}}$ ), X-ray  
 208 ( $f_{1\text{keV}}$ ) and radio ( $f_{5\text{GHz}}$ ) flux densities listed in the online version of the Roma-BZCAT blazar  
 209 catalog (Massaro et al. 2009), and using an empirical relationship between those broadband  
 210 indices and  $\nu_{\text{peak}}^s$  as derived in Abdo et al. (2010d). LSP-BLs have their synchrotron peak at  
 211  $\nu_{\text{peak}}^s < 10^{14}$  Hz, ISP-BLs at  $10^{14} \text{ Hz} \leq \nu_{\text{peak}}^s \leq 10^{15}$  Hz and HSP-BLs at  $\nu_{\text{peak}}^s > 10^{15}$  Hz. This  
 212 is found to be in agreement with the classifications used in Abdo et al. (2010c,d). Nearly  
 213 all the 296 FSRQs are of LSP-type, while only 23% of the 300 BL Lacs are LSP-BLs, 15%  
 214 are ISP-BLs, and 39% are HSP-BLs, 72 AGNs could not be classified, and 41 AGNs are of  
 215 other type than listed above.

216 Redshift information on the sources is extracted from the counterpart source catalogs  
 217 (CRATES, CGRaBS, Roma-BZCAT). While all the redshifts of the 1LAC FSRQs are known,  
 218 only 42% of the high-confidence BL Lacs have measured redshifts. Obviously, AGN without  
 219 redshift information are not used in the present work.

220 The intrinsic average photon indices of *Fermi* blazars in the LAT energy range indicate  
 221 a systematic hardening with source type from  $\sim 2.5$  for FSRQs via  $\sim 2.2$  for LSP- and  
 222  $\sim 2.1$  for ISP-, to  $\sim 1.9$  for HSP-BLs (Abdo et al. 2010c). On the other hand, their redshift  
 223 distributions systematically decrease from the high-redshift (up to  $z \sim 3.1$ ) FSRQs, via  
 224 LSP-BLs located up to a redshift  $z \sim 1.5$ , down to the mostly nearby HSP-BLs at  $z < 0.5$ .  
 225 This mimics a spectral softening with redshift if blazars are not treated separately by source  
 226 type. A search for any systematic spectral evolution must therefore differentiate between  
 227 the various AGN sub-classes (see below).

228 To detect absorption features in the HE spectra of *Fermi* blazars, a thorough under-  
 229 standing of their intrinsic spectra, including variability, and source internal spectral features  
 230 is required. Most blazars do not show strong spectral variability in the LAT energy range on  
 231  $\gtrsim$  week scales (Abdo et al. 2010c), despite often strong flux variability (Abdo et al. 2010g).  
 232 Indeed at least three blazars which turn out to constrain the UV EBL the most (see Sec-  
 233 tion 3.2.1, 3.2.2), show a  $> 99\%$  probability of being variable in flux (using a  $\chi^2$  test) with a  
 234 normalized excess variance of  $\sim 0.02 - 0.2$ . PKS 1502+106 is one of the most constraining  
 235 sources. It displayed an exceptional flare in August 2008 with a factor  $\sim 3$  increase in flux  
 236 within  $\sim 12$  hours (Abdo et al. 2010b). During this flare a flatter (when brighter) spectral

237 shape was evident with an increased curvature towards higher energies and decreasing flux  
 238 level. If the high energy ( $\gtrsim 10$  GeV) photons are emitted during such flare activity, the con-  
 239 straints on the  $\gamma$ -ray opacity would be tighter if only the flare-state spectral data were used.  
 240 Because of limited photon statistics during the flare, however, we use the more conservative  
 241 time averaged spectrum in the present analysis.

242 Absorption in radiation fields internal to the source (e.g., accretion disk radiation, pho-  
 243 ton emission from the broad line region) may cause a systematic break in the  $\gamma$ -ray spectra  
 244 that coincidentally mimics EBL attenuation (Reimer 2007). In the case where such internal  
 245 absorption occurs, its redshift dependence is guaranteed, even in the absence of accretion  
 246 evolution. This is because of the redshifting of that energy where the interaction probability  
 247 is maximum (Reimer 2007). Any technique that explores systematic variation of observables  
 248 (e.g., changes in spectral slope, flux ratios, e-folding cutoff energy) with redshift to single out  
 249 EBL-induced absorption features in blazars with luminous accretion disk radiation (possibly  
 250 indicated by strong emission lines) might therefore suffer from such a bias.

251 All bright strong-line *Fermi* blazars (i.e., *Fermi*-FSRQs and some LSP- and ISP-BLs),  
 252 however, have been found to show spectral breaks already in the 1-10 GeV (source frame)  
 253 range (Abdo et al. 2010c). This is too low in energy to be caused by EBL-attenuation  
 254 for their redshift range  $\lesssim 3$ . Although it is not clear if these breaks are due to internal  
 255 absorption, the spectral softening results in low photon counts at energies  $\gtrsim 10$  GeV where  
 256 EBL absorption is expected. Spectra of all bright HSP-BLs and some ISP-BLs, on the other  
 257 hand, can be well represented by simple power laws without any signs of curvature or breaks.  
 258 This indicates not only do they not have significant internal absorption in the  $\gamma$ -ray band,  
 259 but also the absence of significant EBL absorption, which is expected to be beyond the LAT  
 260 energy range for this nearby ( $z \lesssim 0.5$ ) blazar population.

261 Consequently, as we show in Section 3.1, it remains challenging to quantify EBL ab-  
 262 sorption effects in the LAT energy range based on population studies. On the other hand,  
 263 the determination of the EBL-caused absorption features from individual blazars requires  
 264 bright, high redshift objects with spectra extending to  $\gg 10$  GeV, and we focus on these  
 265 blazars in Section 3.2.

## 266 2.2. GRB sample and potential biases

267 The *Fermi* LAT has detected 11 GRBs from the beginning of its science operation  
 268 (August, 4<sup>th</sup> 2008) until 30 September 2009, 6 of which have redshift measurements. Figure  
 269 2 shows the redshift and highest energy event associated with each of these GRBs. The

270 probability of non-association is extremely small (see Table 1).

271 GRB prompt emission is highly variable and shows signs of spectral evolution, a source  
 272 of systematics to be considered carefully. Our approach in this paper is to restrict ourselves  
 273 to the analysis of small time windows during the GRB emission where the temporal behavior  
 274 does not seem to change significantly.

275 The GRB spectral behavior is well-represented by the Band function (Band et al. 1993)  
 276 in the keV–MeV range. An additional hard,  $\Gamma \sim 1.5$ –2, power-law component, dominating  
 277 at  $\gtrsim 100$  MeV, has now been firmly identified in a few GRBs: GRB090510 (Ackermann et al.  
 278 2010), GRB090902B, (Abdo et al. 2009c), GRB090926A (Abdo et al. 2010h). Its absence  
 279 in other LAT bursts could well be due to limited photon statistics. We assume that the  
 280 power-law component extends well beyond 100 MeV up to  $\sim 10$  GeV, below which EBL  
 281 absorption is negligible. EBL absorption is then expected to soften the power-law spectra  
 282 from the extrapolation of the intrinsic/unabsorbed spectra beyond  $\sim 10$  GeV. Systematic  
 283 effects will, of course, occur when an intrinsic spectrum at high energies differs from this  
 284 extrapolation. Source internal and/or intrinsic absorption via pair creation, e.g., would  
 285 produce a curvature of the spectrum at higher energy which could be misinterpreted as an  
 286 EBL absorption effect. Such a spectral break, which could be due to intrinsic pair creation,  
 287 was detected in the LAT data from GRB 090926A (Abdo et al. 2010h) but we note that a  
 288 corresponding roll-off in the intrinsic spectrum can only make our limits on the  $\gamma$ -ray opacity  
 289 more conservative. By contrast, a rising spectral component above  $>10$  GeV would make our  
 290 limits less constraining, but in the absence of any evidence for inverted gamma-ray spectra  
 291 in GRBs, we consider this possibility unlikely.

### 292 3. Analysis of $\gamma$ -ray Flux Attenuation and Results

293 Assuming that high-energy photon absorption by the EBL is the sole mechanism that  
 294 affects the  $\gamma$ -ray flux from a source at redshift  $z$ , the observed (i.e. absorbed) and unabsorbed  
 295 fluxes at the observed energy  $E$  can be related by the opacity,  $\tau_{\gamma\gamma}(E, z)$ , as

$$F_{obs}(E) = \exp[-\tau_{\gamma\gamma}(E, z)]F_{unabs}(E). \quad (1)$$

296 This is the primary expression that we use to (i) explore  $\gamma$ -ray flux attenuation in the EBL  
 297 from AGNs by means of a redshift-dependent flux ratio between a low- and a high- energy  
 298 band; (ii) constrain EBL models which predict  $\tau_{\gamma\gamma}(E, z)$  values much higher than the opacity  
 299 that would give the observed fluxes from individual blazars and GRBs; and (iii) put upper  
 300 limits on the  $\gamma$ -ray opacity calculated from the observed flux of individual blazars and GRBs,  
 301 and the extrapolation of the unabsorbed flux to high energies. We discuss these methods

302 and the results from our analysis below.

### 303 3.1. Flux ratios - a population based method

304 Because of inherent uncertainties in the determination of the intrinsic spectrum ( $\Gamma_{int}$ )  
 305 for any given blazar in the pre-*Fermi* era, Chen et al. (2004) proposed the average ratio  
 306  $F(> 10 \text{ GeV})/F(> 1 \text{ GeV})$  for all blazars with significant detections above 1 GeV, weighted  
 307 according to the errors in  $F(> 1 \text{ GeV})$ , as a redshift-dependent tracer of the EBL attenuation  
 308 of  $\gamma$ -ray flux. The average flux ratio could then be compared with the predictions of the  
 309 EBL models, taking selection effects into account. This approach assumes that the blazars  
 310 are sampled from a homogeneous distribution with a single redshift-dependent luminosity  
 311 function and a single intrinsic spectral index distribution. Preliminary results from *Fermi*  
 312 (Abdo et al. 2009b) indicate that this assumption is inadequate. Consequently, we have  
 313 calculated the average flux ratios for the different classes of blazars and discuss the results  
 314 below.

315 Among the AGN sample described in Section 2.1 we find that 237 FSRQs, 110 BL Lacs  
 316 and 25 other AGNs are clean<sup>5</sup> 1LAC associations with known redshift and detectable fluxes  
 317 at energies  $\geq 1 \text{ GeV}$ . For 2 BL Lacs the sub-classification is unknown. There are 30 LSP-,  
 318 18 ISP- and 60 HSP- BL Lacs in this sub-sample. For each BL Lac and FSRQ, we calculated  
 319 the ratio between the fluxes above 10 GeV and 1 GeV and their corresponding statistical  
 320 errors following Chen et al. (2004). In 300 of the 372 clean sample sources, only upper limits  
 321 were found for the flux above 10 GeV; in these cases we set the flux equal to one half the  $2\sigma$   
 322 upper limit and the error to the same value.

323 Figure 1 shows the flux ratios for the FSRQ population and BL Lac sub-populations in  
 324 equal redshift bins. The approximately constant distributions of the ratios with redshift at  
 325 small values for the FSRQs and LSP-BL Lacs are due to their soft spectra, with the mean  
 326 values  $\Gamma \sim 2.5$  and  $\Gamma \sim 2.2$ , for the FSRQ and LSP-BL Lac populations respectively. The  
 327 flux ratio is much higher for the HSP-BL Lac populaton because of their hard spectra with  
 328 a mean value  $\Gamma \sim 1.9$ . The large scatter in flux ratio distributions for the HSP-BL Lacs over  
 329 a small redshift range precludes identifying a redshift trend in the ratio. The ISP-BL Lac  
 330 population has a mean spectral index  $\Gamma \sim 2.1$  with an rms fluctuation of 0.22, yielding a  
 331 mean flux ratio between those of the ISP-BL Lacs and the LSP-BL Lacs. Thus the apparent  
 332 discrepancies between the flux ratios for different BL Lac sub-populations arise from the

---

<sup>5</sup>i.e., its association probability is at least 80%, it is the sole AGN associated with the corresponding  $\gamma$ -ray source, and it is not flagged to have problems that cast doubt on its detection (Abdo et al. 2010e)

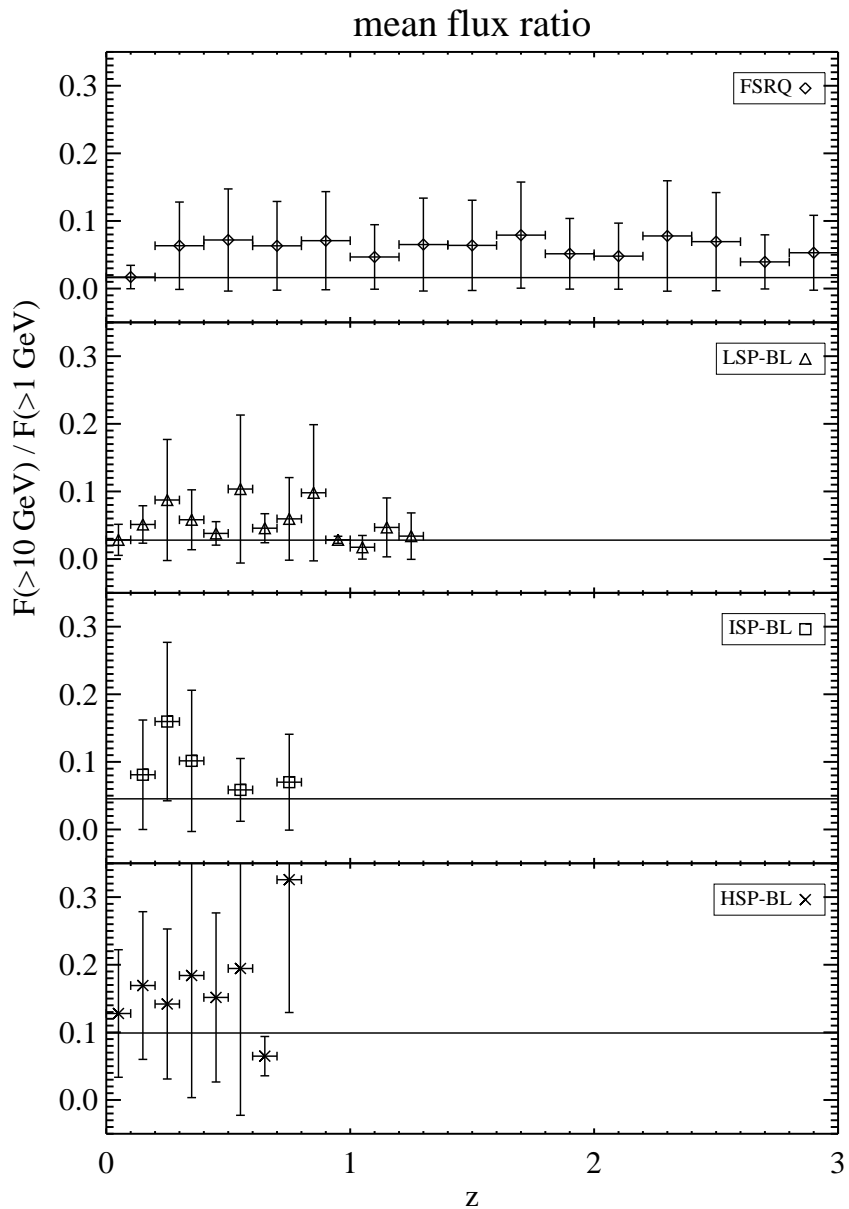


Fig. 1.— Flux ratio  $F(\geq 10 \text{ GeV})/F(\geq 1 \text{ GeV})$  as function of redshift, in the *Fermi* LAT energy range, for FSRQs and BL Lac populations. The horizontal solid lines correspond to the mean ratios (0.016 (FSRQ), 0.028 (LSP-BL), 0.045 (ISP-BL) and 0.099 (HSP-BL)) which were obtained by considering the individual data points rather than the binned averages.

333 fact that the LAT samples different parts of the blazar SED for these sub-classes. Indeed  
 334 a redshift distribution of the flux ratio for the combined BL Lac population would show a  
 335 strong, apparently decreasing trend as would be expected from an EBL absorption effect.

336 Fitting the flux ratios of the FSRQs to a constant as a function of redshift produces a  
 337 value of 0.016 with a reduced  $\chi^2$  of 0.74; a parent distribution with a constant flux ratio would  
 338 produce a lower value with a probability of only  $8.6 \times 10^{-4}$ . We found no significant redshift  
 339 dependence of the flux ratios within the various BL Lac sub-classes. The constant flux ratio  
 340 fits of 0.028 to LSPs and 0.045 to ISPs have a reduced  $\chi^2$  of 0.64 and 0.78, respectively,  
 341 corresponding to probabilities of 0.07 and 0.29. The HSPs have a constant flux ratio of  
 342 0.099 with a reduced  $\chi^2$  of 0.77, corresponding to a probability of 0.10.

343 The flux ratio versus redshift relationship for BL Lacs is therefore primarily due to  
 344 the differing intrinsic spectral characteristics of BL Lacs, rather than from EBL absorption.  
 345 This test is a reminder of the importance of a careful consideration of the intrinsic spectral  
 346 characteristics of the source populations chosen to probe EBL absorption.

### 347 **3.2. Constraints on EBL models from individual source spectra**

348 The sensitivity of the LAT over a broad energy range provides a unique opportunity to  
 349 probe  $\gamma$ -ray spectra from AGNs and GRBs at  $< 10$  GeV where EBL absorption is negligible  
 350 and at  $\gtrsim 10$  GeV where EBL absorption can be substantial. Thus extrapolations of the  
 351 unabsorbed flux at low energies from individual sources to high energies, and assuming that  
 352 the intrinsic spectra do not become harder at high energies, allows us to derive a measure of  
 353 the total absorption (source in-situ and in EBL). Furthermore, since any intrinsic spectral  
 354 curvature or internal absorption effects can not be decoupled from EBL-caused curvature, the  
 355 constraints derived below shall be considered as conservative upper limits on the EBL-caused  
 356 opacity. These are then confronted with various EBL models. Clearly, high EBL density  
 357 models possess a higher probability to be constrained by these methods than low density  
 358 ones. In the following, we use two methods: the highest energy photon (Section 3.2.1) and  
 359 the likelihood (Section 3.2.2) methods.

#### 360 *3.2.1. Highest energy photons*

361 A simple method to constrain a given EBL model is to calculate the chance probability  
 362 of detecting a photon with energy  $E \geq E_{max}$ , where  $E_{max}$  is the energy of the most energetic  
 363 photon that we would expect when the source intrinsic spectrum is folded with the opacity

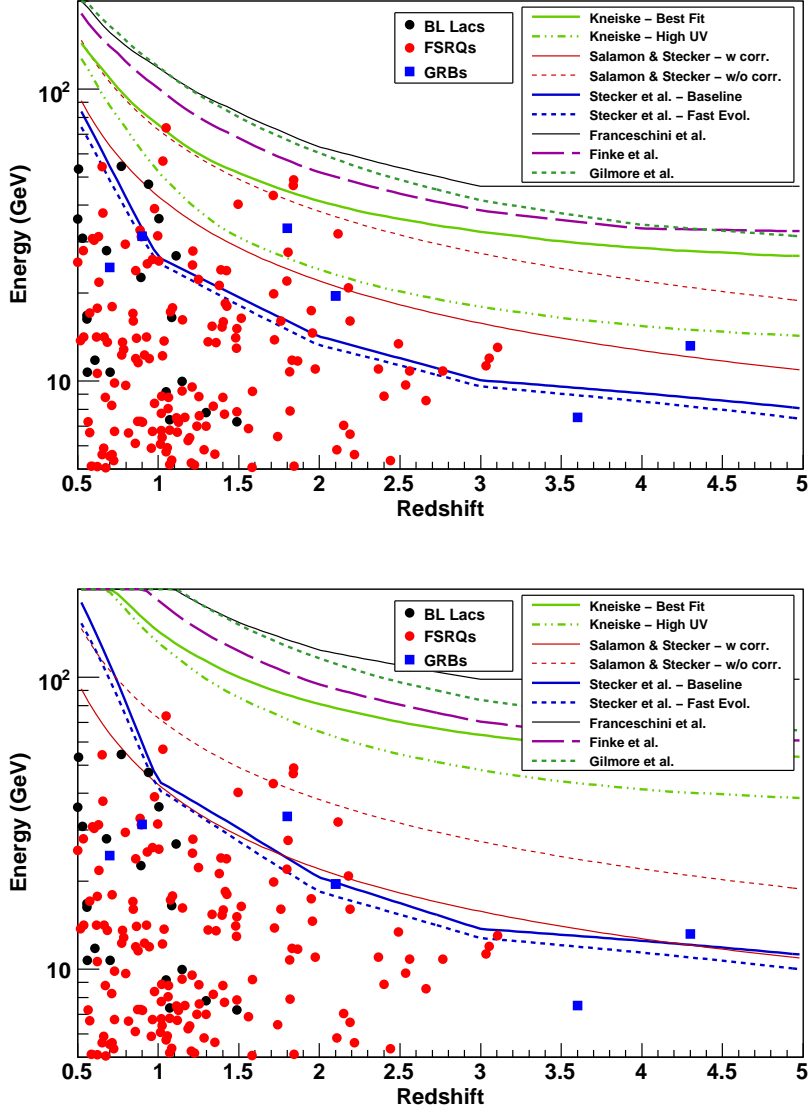


Fig. 2.— Highest-energy photons from blazars and GRBs from different redshifts. Predictions of  $\gamma\gamma$  opacity  $\tau_{\gamma\gamma} = 1$  (top panel) and  $\tau_{\gamma\gamma} = 3$  (bottom panel) from various EBL models are indicated by lines. Photons above model predictions in this figure traverse an EBL medium with a high  $\gamma$ -ray opacity. The likelihood of detecting such photon considering the spectral characteristics of the source are considered in the method presented in section 3.2.1.

Source	$z$	$E_{max}$ (GeV)	Conv. Type	68% radius	Separation	Chance Probability
J1147-3812 (PKS 1144-379)	1.05	73.7	<i>front</i>	0.054°	0.020°	$7.0 \times 10^{-4}$
J1504+1029 (PKS 1502+106)	1.84	48.9	<i>back</i>	0.114°	0.087°	$5.6 \times 10^{-3}$
		35.1	<i>back</i>	0.117°	0.086°	$9.8 \times 10^{-3}$
		23.2	<i>front</i>	0.072°	0.052°	$5.6 \times 10^{-3}$
J0808-0751 (PKS 0805-07)	1.84	46.8	<i>front</i>	0.057°	0.020°	$1.5 \times 10^{-3}$
		33.1	<i>front</i>	0.063°	0.038°	$2.7 \times 10^{-3}$
		20.6	<i>front</i>	0.075°	0.029°	$6.9 \times 10^{-3}$
J1016+0513 (CRATES J1016+0513)	1.71	43.3	<i>front</i>	0.054°	0.017°	$1.2 \times 10^{-3}$
		16.8	<i>front</i>	0.087°	0.035°	$8.2 \times 10^{-3}$
		16.1	<i>front</i>	0.084°	0.018°	$8.2 \times 10^{-3}$
J0229-3643 (PKS 0227-369)	2.11	31.9	<i>front</i>	0.060°	0.035°	$1.7 \times 10^{-3}$
GRB 090902B	1.82	33.4	<i>back</i>	0.117°	0.077°	$6.0 \times 10^{-8}$
GRB 080916C	4.24	13.2	<i>back</i>	0.175°	0.087°	$2.0 \times 10^{-6}$

Table 1: List of blazars and GRBs detected by the LAT which have redshift measurements, and which constrain the EBL opacity the most. For each source, J2000 coordinate based name (other name), the highest-energy photon (HEP), the conversion type, the 68% containment radius (based on the energy and incoming direction in instrument coordinates of the event), the separation from the source and the chance probability of the HEP being from the galactic diffuse or isotropic backgrounds are also listed. The three highest-energy photons are listed for those sources that have multiple constraining photons.

364 from the specific EBL model we want to test. We derive a conservative estimate of the  
 365 intrinsic flux of the source by extrapolating the unabsorbed spectrum at low energies to high  
 366 energies. We consider the LAT spectrum to be representative of the intrinsic spectrum at  
 367 energies where the EBL is supposed to absorb less than  $\sim 1\%$  of the photons for the most  
 368 opaque models. This corresponds to an energy of around 10 GeV (down to  $\sim 6$  GeV for  
 369 GRB 080916C at  $z \sim 4.3$ ). Best fit spectral parameters of this “low-energy” unabsorbed  
 370 spectrum were derived for all sources of the HEP set (see Table 2). The spectrum is assumed  
 371 to be a power law unless a significant deviation from this shape is measured at  $\lesssim 10$  GeV  
 372 (as is indeed observed from, e.g., FSRQs at GeV energies).

373 Iterating through the source list described in Section 2.1 and Section 2.2 we find the  
 374 energy  $E_{\max}$  of the highest-energy photon detected within the 68% containment radius (using  
 375 the specific P6\_V3\_DIFFUSE instrument response functions for *front* and *back* events) of  
 376 each source position. The resulting  $E_{\max}$  versus source redshift is shown in Figure 2 for  
 377 sources with  $z > 0.5$ , and compared to predictions of various EBL models. Evidently, a  
 378 number of events (hereafter *highest-energy photons* or HEP) are populating a region of the  
 379  $E_{max} - z$  phase space where EBL attenuation effects are predicted to be significant. These  
 380 (henceforth called “HEP set”) will be used in the following sections to constrain EBL models  
 381 and to calculate the maximum amount of EBL attenuation that is consistent with the LAT  
 382 observations<sup>6</sup>.

383 It is possible that the high-energy photons considered here may not be emitted in the  
 384 high-redshift source and instead is originated in any of the following background sources:  
 385 Galactic  $\gamma$ -ray diffuse, isotropic (Extragalactic  $\gamma$ -ray plus charged-particle residuals) or a  
 386 nearby point source. The likelihood of detecting any of these background photons within  
 387 the 68% containment radius used to find the HEP set is quantified by computing the number  
 388 of expected events within the 68% containment radius at the location of the source as deter-  
 389 mined by the best fit background model (Galactic and isotropic diffuse + point sources) and  
 390 the instrument acceptance. The last column of Table 1 shows such probability for photons  
 391 in the HEP set. These chance probabilities, although being fairly small are non-negligible  
 392 (at least in the case of blazars) if one would like to set significant constraints on specific  
 393 EBL models by using this HEP. We later describe how this probability for the HEP to be  
 394 a background fluctuation was incorporated in our final results for this method. For now we  
 395 will assume that this HEP is indeed from the source and we will first derive the type of  
 396 constraints it allows us to set on different EBL models. We also note that a stricter set of  
 397 cuts (*extradiffuse*) has been developed by the LAT team to study the Extragalactic  $\gamma$ -ray

---

<sup>6</sup>Only the highest energy photon from each source is plotted in Figure 2. There are a few sources however with more than one constraining photon as indicated in Table 1.

398 background (Abdo et al. 2010f). Despite the decreased  $\gamma$ -ray acceptance we find all photons  
 399 in the HEP set to be retained when using these selection cuts.

400 Monte-Carlo simulations are performed in order to test a particular EBL model with  
 401 the derived intrinsic spectrum absorbed by the EBL as the Null-hypothesis. The simulations  
 402 were performed using *gtobssim*, one of the science tools distributed by the *Fermi* science  
 403 support center and the LAT instrument team. For each simulation we define the unabsorbed  
 404 spectrum of the source as a power law (or *log parabola* in the case of J1504+1029) with  
 405 spectral parameters drawn randomly from the best-fit values (and corresponding uncertainty)  
 406 shown in Table 2. EBL absorption is applied according to the optical depth values of the  
 407 considered model, and finally, the position and orientation of the *Fermi* satellite during the  
 408 time interval described in Section 2 is used to account for the instrument acceptance that  
 409 corresponds to the observations. The highest-energy photon from the simulated data is  
 410 obtained following the exact same cuts and analysis procedure that was used for the data.

411 The resulting distribution of the HEP simulated in each case (see e.g., Figure 3) is used  
 412 to estimate the chance probability of detecting a photon from the source with energy equal  
 413 or greater than  $E_{\max}$ . We produced  $\sim 800000$  and  $\sim 100000$  simulations for each of the HEP  
 414 sets for AGN and for GRBs, respectively. The number of simulations in each case was chosen  
 415 to reach sufficient statistics at the tail of the distribution where the energy of the HEP is  
 416 measured. Distributions of the HEP events from these MC simulations for GRB 080916C  
 417 and GRB 090902B are shown in Figure 4. The open and filled histograms correspond to the  
 418 distributions using the GRB spectra without and with EBL absorption using the “baseline  
 419 model” of Stecker et al. (2006).

420 We applied this analysis to the most constraining sources and using the most opaque  
 421 EBL models. In the end, we find the “baseline” and “fast evolution” models<sup>7</sup> of Stecker et al.  
 422 (2006) to be the only models significantly constrained by our observations. Column 5 of  
 423 Table 3 shows the opacity of the “baseline” of Stecker et al. (2006) for the HEP events.  
 424 In particular we here report on our results for the “baseline” model but we note that the  
 425 “fast evolution” model predicts an even higher opacity to  $\gamma$ -rays so the constraints on this  
 426 model will naturally be higher than the one found for the “baseline” model. Assuming the  
 427 HEP is indeed from the source, the probability of observing such high energy photon given  
 428 the specific EBL model tested (called  $P_{HEP}$ ) is calculated as the ratio between the number

---

<sup>7</sup>The “baseline” model considers the case where all galaxy  $60\mu\text{m}$  luminosities evolved as  $(1+z)^{3.1}$  up to  $z \leq 1.4$ , non-evolving between  $1.4 < z < 6$  and no emission at  $z > 6$ . In contrast, the “fast evolution model” assumes a more rapid galaxy luminosity evolution:  $\propto (1+z)^4$  for  $z < 0.8$ ,  $\propto (1+z)^2$  for  $0.8 < z < 1.5$ , no evolution for  $1.5 < z < 6$ , and no emission at  $z > 6$ . Consequently, for a given redshift the “fast evolution model” predicts a higher  $\gamma$ -ray attenuation than the “baseline model”.

Source	normalization $N_0$ ( $10^{-7}$ ph cm $^{-2}$ s $^{-1}$ MeV $^{-1}$ )	photon index $\Gamma$ (PL)	$\Gamma, \beta, E_b/\text{GeV}$ (LP)	TS
J1147-3812	$0.570 \pm 0.081$	$2.38 \pm 0.09$	...	221
J1504+1029	$(1.84 \pm 0.23) \cdot 10^{-4}$	...	$2.36 \pm 0.03,$ $0.09 \pm 0.01,$ $2.0 \pm 0.1$	34638
J0808-0751	$1.212 \pm 0.078$	$2.09 \pm 0.04$	...	1498
J1016+0513	$1.183 \pm 0.078$	$2.27 \pm 0.05$	...	1220
J0229-3643	$0.789 \pm 0.075$	$2.56 \pm 0.07$	...	394
J1012+2439	$0.552 \pm 0.058$	$2.21 \pm 0.07$	...	443
GRB 090902B	$146 \pm 56$	$1.40 \pm 0.37$	...	1956
GRB 080916C	$1146 \pm 199$	$2.15 \pm 0.22$	...	1398

Table 2: Parameter values of the power law (PL) fits  $dN/dE = N_0(-\Gamma + 1)E^{-\Gamma}/[E_{max}^{-\Gamma+1} - E_{min}^{-\Gamma+1}]$  in the range  $E_{min} = 100$  MeV to  $E_{max} = 10$  GeV of the sources (AGN and GRBs) listed in Table 3 except for source J1504+1029 where a log parabolic parametrization (LP)  $dN/dE = N_0(E/E_b)^{-(\Gamma+\beta \log(E/E_b))}$  has been found to be preferable over a power law fit (with  $\Delta TS = 71.9$ ). The spectral fits for the GRBs are performed below 6 GeV and 3 GeV for GRB 090902B and GRB 080916C, respectively. The TS values are obtained through a likelihood ratio test comparing a model with background only and a model where a point source was added.

429 of cases where the HEP energy is above  $E_{max}$  (actually  $E_{max} - \sigma_{E_{max}}$  given the energy  
430 dispersion) and the total number of simulations performed .

431 To compute the final probability of rejection for the specific EBL model tested (called  
432  $P_{rejection}$ ), one needs to consider the fact that the HEP could be a background photon. We  
433 compute the probability for this to happen in table 1 ( $P_{bkg}$ ). In the end, one can fail to  
434 reject the EBL model because the HEP might be a background event or because there is  
435 a chance for a source photon with energy  $E_{max}$  not to be absorbed by the EBL so that  
436  $P_{rejection} = P_{bkg} + P_{HEP} \times (1 - P_{bkg})$ .

437 In table 4, we list these 3 probabilities for each of our most constraining sources. When  
438 more than one photon is available for a given source, the probabilities are combined resulting  
439 in a stronger rejection. Although  $P_{HEP}$  can be quite constraining, our final significance of  
440 rejection is limited by  $P_{bkg}$  which is non-negligible in the case of blazars and which depends  
441 on the size of the region around each source defined *a priori* to look for associated high-energy  
442 events (68% PSF containment radius in this analysis). A larger HEP acceptance region (90%  
443 or 95% containment radius instead of 68%) would increase the background probability  $P_{bkg}$   
444 while also adding constraining photons to the HEP set. On a source-by-source basis, the  
445 rejection probability goes up or down with increasing radius depending on the number and  
446 energy of these additional photons, but our overall result remains the same. The unbinned  
447 likelihood method, which we describe in the next subsection (3.2.2), does not make use of  
448 an acceptance radius, and instead makes full use of available information in the data to  
449 systematically calculate a model rejection probability.

### 450 3.2.2. Likelihood method

451 This second method to constrain specific EBL models makes use of a Likelihood-Ratio  
452 Test (LRT) technique. This approach compares the likelihood of the Null-hypothesis model  
453 ( $L_0$ ) to best represent the data with the likelihood of a competitive model ( $L_1$ ). The test  
454 statistic (TS) is defined as  $TS = -2 \times (\log(L_0) - \log(L_1))$ . Following Wilks' theorem  
455 (Wilks 1938), the TS is asymptotically distributed as  $\chi_n^2$  (with  $n$  the difference in degrees of  
456 freedom between the two models) if the two models under consideration satisfy the following  
457 two conditions (Protassov et al. 2002): 1) the models must be nested and 2) the null-values  
458 of the additional parameters are not on the boundary of the set of possible parameter values.

459 For the LRT we use the power law intrinsic spectrum convolved with the EBL absorption  
460 predicted by the model ( $\tau_{mod}$ ) we are testing,  $\exp[-\alpha\tau_{mod}(E, z)]F_{unabs}(E)$ , as the observed  
461 flux. For the Null-hypothesis we set  $\alpha = 1$  and we compare it to an alternative model where

Source	$z$	$E_{max}$ (GeV)	$\tau(z, E_{max})$ (F08)	$\tau(z, E_{max})$ (St06, baseline)	Number of photons above 15 GeV
J1147-3812	1.05	73.7	0.40	7.1	1
J1504+1029	1.84	48.9	0.56	12.2	7
J0808-0751	1.84	46.8	0.52	11.7	6
J1016+0513	1.71	43.3	0.39	9.0	3
J0229-3643	2.11	31.9	0.38	10.2	1
GRB 090902B	1.82	33.4	0.28	7.7	1
GRB 080916C	4.24	13.2	0.08	5.0	1

Table 3: Opacity to HEP calculated using the EBL model of Franceschini et al (2008; F08) in comparison to the “baseline” model of Stecker et al. (2006) (St06). Also listed are the number of photons associated to the source which have  $\geq 15$  GeV energy and which can potentially constrain EBL models.

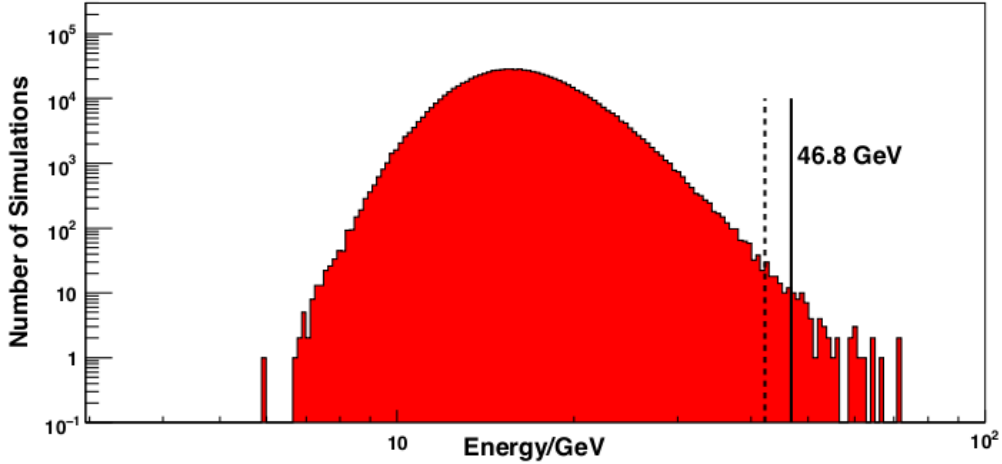


Fig. 3.— Distribution of high-energy photons obtained from Monte-Carlo simulations of the source J0808-0751 with the EBL attenuation by Stecker et al. (2006).  $E_{max}$  and  $E_{max} - \sigma_{E_{max}}$  (where  $\sigma_{E_{max}}$  is the energy uncertainty) are indicated by a solid and dotted vertical black lines, respectively. The probability of detecting a photon with energy equal or greater to  $E_{max} - \sigma_{E_{max}}$  is equal to  $6.8 \times 10^{-5}$ .

Source	$z$	Energy (GeV)	$P_{bkg}$	HEP method applied to Stecker 06		HEP Rejection Significance
				$P_{HEP}$	$P_{rejection}$	
J1147-3812	1.05	73.7	$7.0 \times 10^{-4}$	$1.2 \times 10^{-4}$	$8.1 \times 10^{-4}$	$3.2 \sigma$
J1504+1029	1.84	48.9	$5.6 \times 10^{-3}$	$6.7 \times 10^{-5}$	$5.7 \times 10^{-3}$	$4.1 \sigma$
		35.1	$9.8 \times 10^{-3}$	$6.8 \times 10^{-3}$	$1.7 \times 10^{-2}$	
		23.2	$5.6 \times 10^{-3}$	$1.8 \times 10^{-1}$	$1.9 \times 10^{-1}$	
Combined $P_{rej} = 1.7 \times 10^{-5}$						
J0808-0751	1.84	46.8	$1.5 \times 10^{-3}$	$1.9 \times 10^{-4}$	$1.7 \times 10^{-3}$	$4.5 \sigma$
		33.1	$2.7 \times 10^{-3}$	$3.7 \times 10^{-3}$	$6.4 \times 10^{-3}$	
		20.6	$6.9 \times 10^{-3}$	$2.5 \times 10^{-1}$	$2.6 \times 10^{-1}$	
Combined $P_{rej} = 2.8 \times 10^{-6}$						
J1016+0513	1.71	43.3	$1.1 \times 10^{-3}$	$5.4 \times 10^{-4}$	$1.6 \times 10^{-3}$	$3.3 \sigma$
		16.8	$8.2 \times 10^{-3}$	$4.9 \times 10^{-1}$	$4.9 \times 10^{-1}$	
		16.1	$8.2 \times 10^{-3}$	$6.5 \times 10^{-1}$	$6.5 \times 10^{-1}$	
Combined $P_{rej} = 5.3 \times 10^{-4}$						
J0229-3643	2.11	31.9	$1.7 \times 10^{-3}$	$8.9 \times 10^{-5}$	$1.8 \times 10^{-3}$	$2.9 \sigma$
GRB 090902B	1.82	33.4	$2 \times 10^{-6}$	$2.0 \times 10^{-4}$	$2.0 \times 10^{-4}$	$3.7 \sigma$
GRB 080916C	4.24	13.2	$8 \times 10^{-8}$	$6.5 \times 10^{-4}$	$6.5 \times 10^{-4}$	$3.4 \sigma$

Table 4: Listed are the significance of rejecting the “baseline” model (Stecker et al. (2006)), calculated using the HEP method as described in Section 3.2.1. For completeness, we also report individually the probability of the HEP to be a background event ( $P_{bkg}$ ) and the probability for this HEP not to be absorbed by the EBL if it were emitted by the source ( $P_{HEP}$ ). As explained in the text:  $P_{rejection} = P_{bkg} + P_{HEP} \times (1 - P_{bkg})$ . For those sources with more than one constraining photon, the individual and combined  $P_{rejection}$  are calculated. The “fast evolution” model by Stecker et al. (2006) is more opaque and leads to an even higher significance of rejection. Applying this method to less opaque models leads to no hints of rejection since the probability  $P_{HEP}$  is large in those cases (e.g.  $\gtrsim 0.1$  for the Franceschini et al. (2008) EBL model). Note that a log parabola model was used as the intrinsic model for source J1504+1029 since evidence of curvature is observed here even below 10 GeV (see Table 2).

462  $\alpha$  is left as a free parameter, which therefore has one more degree of freedom than the Null-  
 463 hypothesis. In the absence of any flux attenuation by the EBL,  $\alpha = 0$ . Note that we allow  
 464 the normalization parameter,  $\alpha$  to go to negative values. This choice, although not physically  
 465 motivated, allows us to satisfy the second condition mentioned above. As a consequence the  
 466 Test-Statistics can simply be converted into a significance of rejecting the Null-hypothesis by  
 467 making use of Wilks’ theorem. Because of the lack of information on the intrinsic spectrum  
 468 of a distant source above 10 GeV, we use the (unabsorbed)  $\leq 10$  GeV observed spectrum as  
 469 a reasonable assumption for the functional shape of the intrinsic source spectrum. A simple  
 470 power law was found to be a good fit to the  $\leq 10$  GeV data for the sources listed in Table 3  
 471 except in the case of J1504+1029 where a log-parabolic spectrum was preferred. We note  
 472 that if the actual intrinsic curvature is more pronounced than the one found with the best  
 473 fit below 10 GeV, this would only make the results more constraining.

474 As we mentioned earlier, although we are considering all EBL models in the literature,  
 475 we find that our observations are only constraining the most opaque ones. Figure 5 shows  
 476 the TS value as a function of the opacity normalization parameter  $\alpha$ , for the three most con-  
 477 straining blazars (J1016+0513, J0808-0751, J1504+1029) and the two GRBs (GRBs 090902B  
 478 and 080916C) when considering the “baseline” model of Stecker et al. (2006) with the LRT  
 479 method. All sources are found to have an opacity normalization parameter that is consistent  
 480 with  $\alpha \geq 0$  at the  $1\sigma$  level which is reassuring as we do not expect a rise in the spectrum on a  
 481 physical basis.  $\sqrt{TS}$  for  $\alpha = 1$  corresponds to the rejection significance for the specific model  
 482 considered. The most constraining source, J1016+0513 rejects the Null-hypothesis ( $\alpha = 1$ ,  
 483 corresponding to the baseline model of Stecker et al. (2006) in this case) with a significance  
 484 of  $\sim 6.0\sigma$ . This source could also constrain the “high UV model” of Kneiske et al. (2004)  
 485 with a significance of  $3.2\sigma$  although multi-trials effect substantially reduce this significance  
 486 (see Section 3.2.3).

487 As compared to the HEP method, the LRT method incorporates the possibility of each  
 488 photon being from the background into the unbinned maximum likelihood computation.  
 489 Thus separate calculations of the background probability and corresponding rejection proba-  
 490 bility are not needed. Also since the LRT method takes into account all high-energy photons  
 491 rather than the highest-energy ones in the HEP method, it gives more constraining results  
 492 for EBL model rejection with the exception of 2 GRBs where HEP method gives slightly  
 493 more constraining results. Finally, we note that the *a priori* choice of the size of the region  
 494 around each source defined to look for associated high-energy events is a source of systemat-  
 495 ics for the HEP method ( which uses 68% PSF containment radius) while it does not affect  
 496 the LRT method.

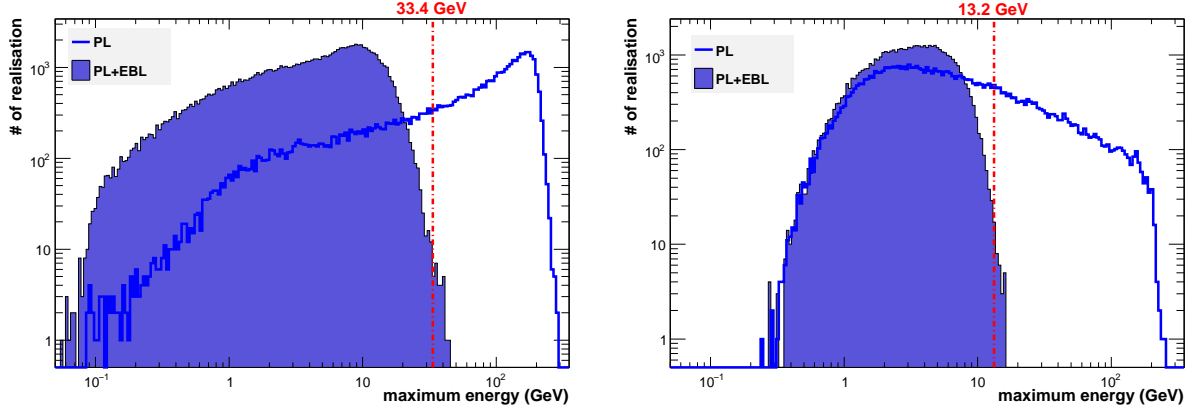


Fig. 4.— Distributions of the highest energy photons from simulations performed with estimates of our intrinsic spectra for GRB 080916C (left panel) and GRB 090902B (right panel), folded with EBL attenuation calculated using the Stecker et al. (2006) baseline model. The total number of realizations ( $10^5$ ) in both the power-law and power-law convolved with the EBL cases is the same.

Source	$z$	LRT Rejection Significance	
		pre-trial	post-trial
J1147-3812	1.05	$3.7\sigma$	$2.0\sigma$
J1504+1029	1.84	$4.6\sigma$	$3.3\sigma$
J0808-0751	1.84	$5.4\sigma$	$4.4\sigma$
J1016+0513	1.71	$6.0\sigma$	$5.1\sigma$
J0229-3643	2.11	$3.2\sigma$	$1.2\sigma$
GRB 090902B	1.82	$3.6\sigma$	$1.9\sigma$
GRB 080916C	4.24	$3.1\sigma$	$1.0\sigma$

Table 5: Significance of rejecting the “baseline” model (Stecker et al. (2006)), calculated using the LRT method described in Section 3.2.2. Again, the “fast evolution” model by Stecker et al. (2006) leads to a high rejection significance with two sources (J0808-0751 and J1016+0513) with  $> 4\sigma$  post-trial significance. The post-trial significance is computed by taking into account the fact that our analysis is considering  $\sim 200$  independent sources.

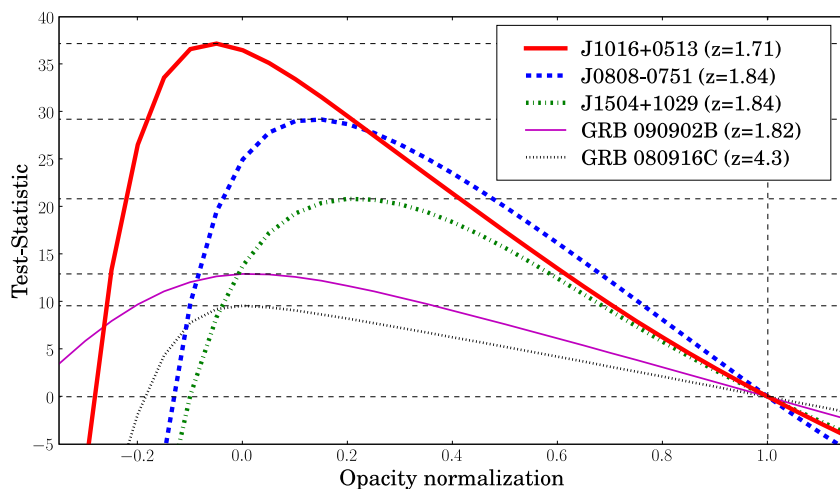


Fig. 5.— Test statistic (TS) as a function of the opacity normalization parameter calculated from the likelihood ratio test (LRT) for J1016+0513, J0808-0751, J1504+1029 and GRBs 090902B and 080916C. The "baseline" model of Stecker et al. (2006) has been used and the rejection for this model can be directly read out as  $\Delta TS$  between  $\alpha = 1$  and the best fit  $\alpha$  for the source (horizontal dashed line). The confidence interval for the normalization parameter can be obtained using  $\Delta TS = CL^2$  where  $CL$  is the confidence level.

3.2.3. *Multi-trial effects and combined probabilities*

Because the search for EBL signatures or rejection of specific EBL models is performed on all blazars and GRBs detected by the LAT, one has to consider multi-trials, which is potentially affecting our analysis. For independent searches, as is the case here, the post-trial probability threshold for obtaining a  $4\sigma$  result is  $P_{\text{post-trial}} = 1 - (1 - P_{4\sigma})^{1/N_{\text{trials}}}$ , where  $N_{\text{trials}}$  is the number of trials and  $P_{4\sigma}$  is the  $4\sigma$  probability threshold for a single search ( $\approx 6.3 \times 10^{-5}$ ). In the present case, the LAT AGN catalog that we have used (Abdo et al. 2010e) includes 709 AGNs of which  $\sim 200$  have a sufficiently high redshift ( $\sim 100$  with  $\gtrsim 10$  GeV photon) to allow for the testing of EBL attenuation models with their  $\gamma$ -ray spectra. Only a handful of LAT GRBs were observed with sufficient statistics to hope to constrain the EBL. In the end, we have  $N_{\text{trials}} \sim 200$  which corresponds to a post-trial probability for a  $4\sigma$  results of  $P_{4\sigma, \text{post-trial}} \approx 3.17 \times 10^{-7}$ . This corresponds to a significance of  $\approx 5.11\sigma$  on an individual source which we will therefore consider as our threshold for a  $4\sigma$  post-trials rejection significance for any specific EBL model. This  $P_{4\sigma, \text{post-trial}}$  threshold was reached in case of Stecker et al. (2006) “baseline” model for sources J0808-0751 and J1016+0513 using the LRT method. Note that J1504+1029 is only slightly below this threshold.

Combining specific EBL model rejection probabilities from multiple sources<sup>8</sup> we get a much higher rejection significance. For HEP probabilities the combined rejection significance for Stecker et al. (2006) “baseline” model is  $\approx 10.8\sigma$  ( $\approx 9.3\sigma$  without the 2 GRBs) from taking product of the probabilities from individual sources. For the LRT method, we add the individual likelihood profiles to derive an overall significance of  $11.4\sigma$  for the same EBL model. Therefore both methods give very large rejection significance even after taking multi-trial effect into account. Since Stecker et al. (2006) “fast-evolution” model gives opacities larger than the “baseline model” in the LAT range, both models can be rejected by our analysis with very high confidence level. All other models can not be significantly rejected even after such stacking procedure is applied.

**3.3. Opacity upper limits**

With a measured flux,  $F_{\text{obs}}$ , at (observed) energy  $E \geq 10$  GeV, and an estimated flux,  $F_{\text{unabs}}$ , also at  $E \geq 10$  GeV, calculated by extrapolating the unabsorbed flux below 10 GeV to these energies, the  $\gamma$ -ray opacity can be estimated as:

---

<sup>8</sup>since the spectral fits of all the sources we considered in this analysis are independent to each other

$$\tau_{\gamma\gamma}(E, z) = \ln[F_{unabs}(E)/F_{obs}(E)]. \quad (2)$$

528 Since the extrapolation gives a maximum value for  $F_{unabs}(E)$ , the opacity,  $\tau_{\gamma\gamma}(E, z)$ , is an  
 529 upper limit, accounting for EBL-caused and any possible intrinsic absorption effects.

530 A maximum likelihood analysis (Mattox et al. 1996) has been used to reconstruct the  
 531 observed source flux  $F_{obs}$ <sup>9</sup>. The same method has also been used to fit the unabsorbed flux  
 532  $F_{unabs}$  and its uncertainty at low energy ( $< 10\text{GeV}$ ) with a PL or a log-parabola function,  
 533 and to extrapolate  $F_{unabs}$  to higher energy by propagating the parameter uncertainties. The  
 534 low energy fit for all the sources was performed with a power law with the exception of  
 535 J1504+1029, which was fitted with a log parabola.

536 To evaluate both  $F_{unabs}$  and  $F_{obs}$ , a model is assumed for the diffuse background flux  
 537 components. The Galactic diffuse emission is modeled using a *mapcube* function, while a  
 538 tabulated model is used for the isotropic component, representing the extragalactic emission  
 539 as well as the residual instrumental background<sup>10</sup>. Both diffuse components are assigned a  
 540 free normalization for the likelihood fit. For the evaluation of the unabsorbed flux,  $F_{unabs}$ ,  
 541 each source within a  $10^\circ$  radius of the source under consideration is modeled with a power  
 542 law where the photon index is fixed to the value from the 1FGL catalog (Abdo et al. 2010i)  
 543 and the integral flux parameter is left free. The remaining sources in a region from  $10^\circ$  to  
 544  $15^\circ$  from the source are modeled by a power law with all spectral parameters fixed. The  
 545 source under study has all spectral parameters free.

546 To measure the observed flux  $F_{obs}$ , the whole energy range is divided in equal logarithmi-  
 547 cally spaced bins, according to the photon statistics of the specific source: 3 bins per decade  
 548 above 10 GeV for J0229-3643 and J1147-3812, 3 bins/dec for J1016+0513, 4 bins/dec for  
 549 J0808-0750 and 5 bins/dec for J1504+1029. In each bin the *gtlike* tool is applied assuming  
 550 for all the sources (all are point-like) a simple power law spectrum with photon index fixed  
 551 to 2.0, while all the integral fluxes of nearby sources (within  $10^\circ$ ) are left as free parameters  
 552 in the fitting procedure (while sources between  $10^\circ$  and  $15^\circ$  are still included but have their  
 553 parameters fixed to the value derived in the 1FGL catalog). In this way, assuming that in  
 554 each energy bin the spectral shape can be approximated with a power law, the flux of the  
 555 source in that bin is derived. Again, the diffuse background components are modeled with  
 556 one single parameter each, i.e., its normalization. The efficiency of this method increases as  
 557 the width of the bins is decreased, however, smaller bins reduce photon statistics per bin

---

<sup>9</sup>*gtlike* tool in the standard *Fermi* LAT *Science Tools* package provided by the *Fermi* Science Support Center (FSSC)

<sup>10</sup><http://fermi.gsfc.nasa.gov/ssc/data/access/lat/BackgroundModels.html>

558 and this could lead to an unreliable fit.

559 Once both  $F_{unabs}$  and  $F_{obs}$  are determined, the maximum opacity in each energy bin can  
 560 be estimated from equation (2). In order to increase the photon statistics in the energy bins  
 561 above 10 GeV, bin sizes for evaluating  $\tau_{\gamma\gamma}$  have been increased where required. An upper  
 562 limit on  $\tau_{\gamma\gamma}(\langle E \rangle, z)$  with 95% CL in a constraining energy bin with mean energy  $\langle E \rangle$  is then  
 563 calculated by propagating the parameter uncertainties in the fitted flux. The opacity upper  
 564 limits calculated from this method at the highest-energy bin  $\langle E_{max} \rangle$  are conservative, and  
 565 only an unlikely hardening of the intrinsic spectra at  $\gtrsim 50$  GeV would invalidate our results.  
 566 We compare these opacity limits with opacities predicted by various EBL models.

567 In Figure 6 (upper left) we show the upper limit (95% CL) derived for the high-energy  
 568 photon detected by the LAT from blazar J0808-0751 at  $z = 1.84$  as an example. A larger  
 569 optical depth would require an intrinsic spectrum that at high energies lies significantly above  
 570 the extrapolation obtained from the low energy spectrum. The figure shows that the upper  
 571 limit rules out those EBL models that predict strong attenuation. This result is consistent  
 572 with all other upper limits derived with this method (see Figure 6 and Table 6).

#### 573 4. Discussion

574 Studies with the highest energy extragalactic photons seen by the *Fermi* LAT primarily  
 575 probe the UV and optical components of the EBL. The background fields responsible for  
 576  $\gamma$ -ray attenuation can evolve strongly with redshift. In many of the models analyzed in this  
 577 paper the EBL intensity can exceed the local value by a factor of 10 or more at redshifts near  
 578 the peak of star-formation rate density. For sources at cosmological distances, the optical  
 579 depth to  $\gamma$  rays created by the EBL is therefore determined by integrating the EBL intensity  
 580 along the line of sight to the source from the observer.

581 For an interaction angle of  $\theta = \pi$ , the electron-positron pair production threshold con-  
 582 dition leads to the value of the longest wavelength photon with which a  $\gamma$ -ray emitted at  $z_{src}$   
 583 with observed energy  $E_{obs}$  can interact (source frame):

$$\lambda_{max} = 47.5 (1 + z_{src}) \left[ \frac{E_{obs}}{\text{GeV}} \right] \text{ \AA} . \quad (3)$$

584 The equation describes an upper limit on background photon wavelengths that can  
 585 contribute to the  $\gamma$ -ray optical depth. Limits for  $\lambda_{max}$  include 7175  $\text{\AA}$  for blazar J1147-3812,  
 586 and 4474  $\text{\AA}$  for GRB 090902B and 3286  $\text{\AA}$  for GRB 080916C, based on the highest-energy  
 587  $\gamma$ -rays seen from these sources. In reality, interactions with shorter wavelength photons are

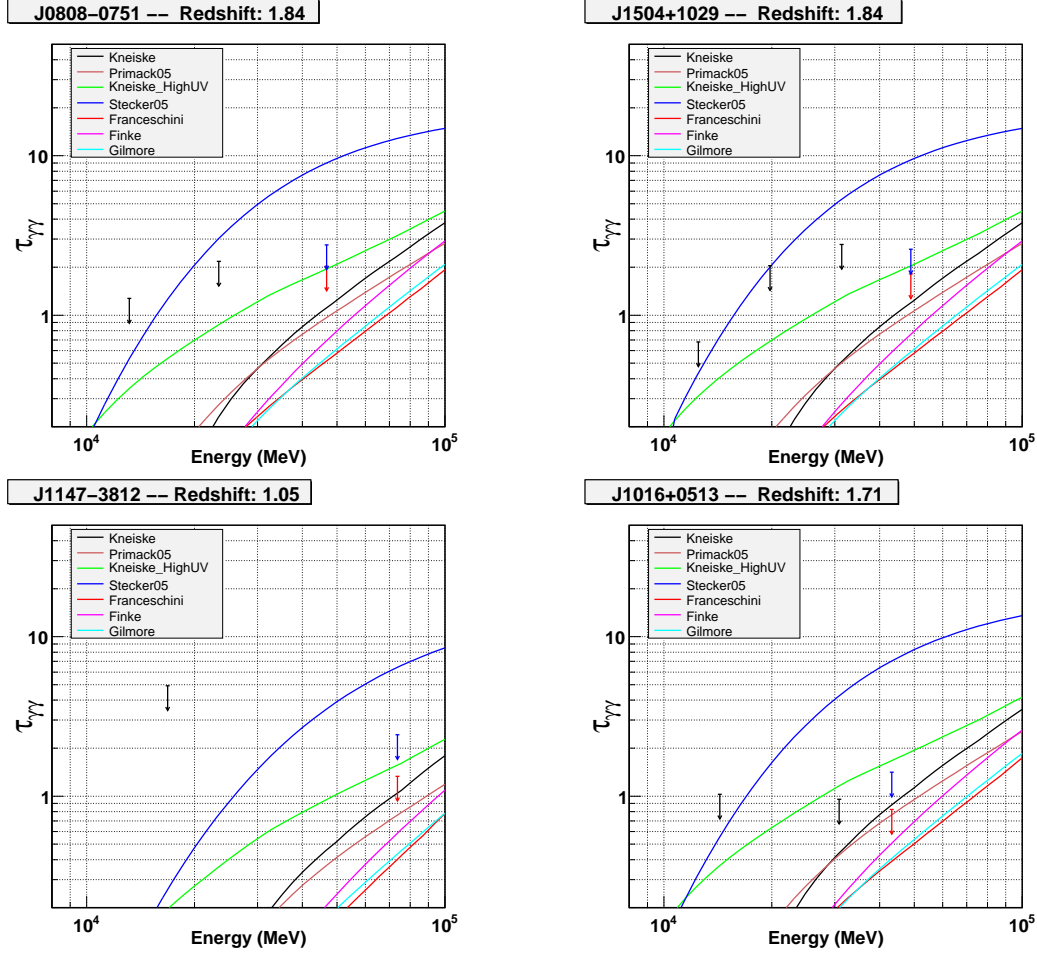


Fig. 6.— Derived upper limits for the optical depth of  $\gamma$ -rays emitted at  $z=1.84$  (J0808-0751, J1504+1029),  $z=1.05$  (J1147-3812) and  $z=1.71$  (J1016+0513). Black arrows: upper limits at 95% c.l. in all energy bins used to determine the observed flux above 10 GeV. Red arrow: upper limits at 95% c.l. for the highest energy photon. Blue arrow: upper limit at 99% c.l. for the highest energy photon. The upper limits are inconsistent with the EBL models that predict the strongest opacity.

588 more likely and will contribute more to the optical depth due to the redshifting of the  $\gamma$ -  
 589 ray during propagation to Earth, the cross section, which peaks at approximately twice the  
 590 threshold energy, and the geometry (interactions at angles of  $\sim 90^\circ$  are more likely than  
 591 head-on interactions as used in Eq. 3).

592 The results of our analysis of the highest energy  $\gamma$ -rays from blazars and GRBs detected  
 593 by the *Fermi* LAT disfavor a UV background intensity at the level predicted both by the  
 594 baseline and fast-evolution models of Stecker et al. (2006), although the LAT observations  
 595 discussed here do not constrain the predictions of this work at longer wavelengths. The  
 596 two models of this work are based upon a backwards evolution model of galaxy formation.  
 597 In this scenario, the IR SED of a galaxy is predicted from its luminosity at  $60 \mu\text{m}$ . The  
 598 locally-determined  $60 \mu\text{m}$  luminosity function is then assumed to undergo pure luminosity  
 599 evolution following a power law in  $(1+z)$ . Optical and UV luminosities, relevant to *Fermi*'s  
 600 extragalactic observations, are then determined by analytic approximation to the SEDs in  
 601 Salamon & Stecker (1998) and are normalized to the short wavelength portions of the IR  
 602 SEDs. These models do not include absorption of UV light by dust in star-forming regions  
 603 and the interstellar medium of galaxies, which may partially account for the high background  
 604 in this model. While this model does account for redshift evolution in the UV-optical SEDs  
 605 of galaxies, it does not allow for any evolution in the IR emission to which these SEDs are  
 606 normalized. As mentioned by Stecker et al. (2006), this is another factor which could result  
 607 in overpredicted UV emission.

608 Emissivity at UV wavelengths is closely tied to the global star-formation rate density.  
 609 Because the models of Stecker et al. (2006) are not derived from an assumed function for  
 610 the star-formation rate, limits on the UV emissivity in this case cannot be used to directly  
 611 constrain star-formation. We do not find that our results are conclusively in disagreement  
 612 with the ‘best-fit’ model of Kneiske et al. (2004) In these models, the optical-UV EBL is  
 613 based upon a Salpeter IMF and a star-formation rate density that peaks at  $z \sim 1.25$ , with  
 614 a value of  $\sim 0.2 \text{ M}_\odot \text{ Mpc}^{-3} \text{ yr}^{-1}$ , and falls slowly towards higher redshift. In the high-UV  
 615 model, ultraviolet flux is boosted by a factor of 4 above the level of the best-fit model, greatly  
 616 enhancing the opacity for  $\gamma$ -rays at energies below about 200 GeV. A star formation history  
 617 of the magnitude required to produce the background in the high-UV model would be above  
 618 essentially all estimates of the global star formation rate (see for example Hopkins & Beacom  
 619 (2006)). All other EBL models are of such low density in the UV range that they can not  
 620 be constrained by the data presented in this work. Although the results of our analysis can  
 621 not yet place any stringent upper limits on the cosmological star-formation history that are  
 622 competitive with current observational estimates, future prospects for probing low density  
 623 UV models of the EBL by means of improved methods and enlarged GeV photon data sets  
 624 may be promising.

625 High-energy  $\gamma$  rays that are absorbed by the EBL photons can initiate a pair cascade by  
 626 subsequent Compton scattering of the CMB photons by the pairs. In case the intergalactic  
 627 magnetic field (IGMF) is very weak, so that the pairs do not deflect out of our line of sight,  
 628 this cascade radiation component can be detectable (Plaga 1995). Calculations of such  
 629 cascade signatures have been carried out for AGNs (see e.g. Dai et al. 2002; Murase et al.  
 630 2008; Essey & Kusenko 2010) and for GRBs (see e.g. Dai & Lu 2002; Razzaque et al. 2004;  
 631 Takahashi et al. 2008) and found to contribute to the observed  $\gamma$ -ray flux even if the  $\tau_{\gamma\gamma}$   
 632 opacity is large. If blazars or GRBs are sources of ultrahigh energy cosmic rays (UHECRs),  
 633 then photohadronic interactions by protons during their propagation in the background  
 634 light can also induce a high-energy cascade signature that would form appreciable high-  
 635 energy emission, provided the IGM magnetic field is sufficiently small (?). However recent  
 636 upper-limits calculated in the *Fermi* LAT range from TeV blazars 1ES 0347-121 and 1ES  
 637 0229+200 constrain the IGMF to be  $> 3 \times 10^{-16}$  G (Neronov & Vovk 2010). Such a strong  
 638 field reduces the cascade flux significantly and the contribution to the observed flux is likely  
 639 to be small.

640 Exotic scenarios involving oscillation between  $\gamma$ -rays and axionlike particles, while prop-  
 641 agating in the Galactic magnetic field, from distant sources may produce observable signa-  
 642 tures in the TeV range (see e.g. Mirizzi et al. 2007; Serpico 2009). However the effect may  
 643 not set in for typically assumed IGMF values or likely to be too small to make up for EBL  
 644 flux attenuation in the  $\gtrsim 100$  GeV range (see e.g. Sanchez-Conde et al. 2010)

## 645 5. Conclusion

646 Using the high-energy 11-month photon data set collected by *Fermi* from distant blazars,  
 647 and two GRBs we have (i) constrained the opacity of the universe to  $\gamma$  rays in the  $\sim 10$ –  
 648 100 GeV range coming from various redshifts up to  $z \approx 4.3$ ; and (ii) ruled out an EBL  
 649 intensity in the redshift range  $\sim 1$  to 4.3 as great as that predicted by Stecker et al. (2006)  
 650 in the ultraviolet range at more than  $4\sigma$  post trials in two independent sources (blazars).  
 651 The overall rejection significance is found to be  $> 10\sigma$  post trials therefore making this  
 652 result very robust. Our most constraining sources are blazars J1504+1029, J0808-0751 and  
 653 J1016+0513 with  $(z, \langle E_{max} \rangle)$  combinations of (1.84, 48.9 GeV), (1.84, 46.8 GeV) and (1.71,  
 654 43.3 GeV), respectively. Although a likelihood ratio analysis of the latter source indicates  
 655 that the sensitivity of our analysis method is approaching the EBL flux level of the “high UV  
 656 model” of Kneiske et al (2004), multi-trial effects markedly reduced the rejection significance.  
 657 The two most constraining GRBs are GRB 090902B and GRB 080916C, both of which rule  
 658 out the Stecker et al. (2006) EBL models in the UV energy range at more than  $3\sigma$  level. We

659 have also calculated model-independent opacity upper-limits  $\tau_{\gamma\gamma,UL}(z, \langle E_{max} \rangle)$  at 95% CL in  
 660 the redshift  $z \simeq 1 - 2.1$  and  $E_{max} \approx 28 - 74\text{GeV}$  ranges.

661 As the high-energy photon data set collected by *Fermi* grows in future and more blazars  
 662 and GRBs are detected at constraining energies, the  $(E, z)$  phase space that constrains  $\tau_{\gamma\gamma}$   
 663 will become more populated. This will provide us with unique opportunities to constrain  
 664 the opacity of the Universe to  $\gamma$ -rays over a large energy and redshift range, and eventually  
 665 help us further understand the evolution of the intensity of the extragalactic background  
 666 light over cosmic time.

667 The *Fermi* LAT Collaboration acknowledges generous ongoing support from a number  
 668 of agencies and institutes that have supported both the development and the operation of the  
 669 LAT as well as scientific data analysis. These include the National Aeronautics and Space  
 670 Administration and the Department of Energy in the United States, the Commissariat à  
 671 l’Energie Atomique and the Centre National de la Recherche Scientifique / Institut National  
 672 de Physique Nucléaire et de Physique des Particules in France, the Agenzia Spaziale Italiana  
 673 and the Istituto Nazionale di Fisica Nucleare in Italy, the Ministry of Education, Culture,  
 674 Sports, Science and Technology (MEXT), High Energy Accelerator Research Organization  
 675 (KEK) and Japan Aerospace Exploration Agency (JAXA) in Japan, and the K. A. Wallen-  
 676 berg Foundation, the Swedish Research Council and the Swedish National Space Board in  
 677 Sweden. Additional support for science analysis during the operations phase is gratefully  
 678 acknowledged from the Istituto Nazionale di Astrofisica in Italy and the Centre National  
 679 d’Études Spatiales in France. The *Fermi* GBM collaboration acknowledges support for  
 680 GBM development, operations and data analysis from NASA in the US and BMWi/DLR in  
 681 Germany. L. Reyes acknowledges support by the Kavli Institute for Cosmological Physics  
 682 at the University of Chicago through grants NSF PHY-0114422 and NSF PHY-0551142 and  
 683 an endowment from the Kavli Foundation and its founder Fred Kavli. AR acknowledges  
 684 support by Marie Curie IRG grant 248037 within the FP7 Program.

685 **REFERENCES**

686 Abdo, A. A., et al. 2009a, *Science*, 323, 1688  
 687 Abdo, A. A., et al. 2009b, *ApJ*, 700, 597  
 688 Abdo, A. A., et al. 2009c, *ApJ*, 706, L138  
 689 Abdo, A. A., et al. 2010a, *ApJ*, 708, 1310

- 690 Abdo, A. A., et al. 2010b, *ApJ*, 710, 810
- 691 Abdo, A. A., et al. 2010c, *ApJ*, 710, 1271
- 692 Abdo, A. A., et al. 2010d, accepted; arXiv:0912.2040
- 693 Abdo, A. A., et al. 2010e, 715, 429
- 694 Abdo, A. A., et al. 2010f, *Phys. Rev. Lett.*, 104, 101101
- 695 Abdo, A. A., et al. 2010g, submitted; arXiv:1004.0348
- 696 Abdo, A. A., et al. 2010h, in prep.: “Detection of a spectral cutoff in the extra hard compo-  
697 nent from GRB 090926A”
- 698 Abdo, A. A., et al. 2010i, accepted: “Fermi Large Area Telescope First Source Catalog”
- 699 Abdo, A. A., et al. 2010j, *ApJ*, 707, 1310
- 700 Acciari, V. A., et al. 2010, *ApJ*, 708, L100
- 701 Ackermann, M., et al. 2010, *ApJ*, accepted
- 702 Aharonian, F. A., et al. 1999, *A&A*, 349, 11
- 703 Aharonian, F. A., et al., 2002, *A&A*, 384, 23
- 704 Aharonian, F. A., et al. 2006, *Nature*, 440, 1018
- 705 Aharonian, F. A., Khangulyan, D., & Costamante, L. 2008, *MNRAS*, 387, 1206
- 706 Albert, J. et al. 2008, *Sci*, 320, 1752
- 707 Atwood, W. B., et al. 2009, *ApJS*, 697, 1071
- 708 Bloom, J., et al. 2009, *ApJS*, 691, 723
- 709 Böttcher, M., Dermer, C. D., & Finke, J. D. 2008, *ApJ*, 679, L9
- 710 Chen, A., Reyes, L. C., & Ritz, S. 2004, *ApJ*, 608, 686
- 711 Costamante, L., Aharonian, F., Horns, D., Ghisellini, G., 2004, *NewAR*, 48, 469
- 712 Dai, Z. G., & Lu, T. 2002, *ApJ*, 580, 1013
- 713 Dai, Z. G., Zhang, B., Gou, L. J., Mészáros, P., & Waxman, E. 2002, *ApJ*, 580, L7

- 714 Driver, S. P., Popescu, C. C., Tuffs, R. J., Graham, A. W., Liske, J., & Baldry, I. 2008, *ApJ*,  
715 678, L101
- 716 Essey, W. & Kusenko, A. 2010, *Astropart. Phys.* 33, 81
- 717 Fazio, G. G., & Stecker, F. W. 1970, *Nature*, 226, 135
- 718 Finke, J. D., & Razzaque, S. 2009, *ApJ*, 698, 1761
- 719 Finke, J. D., Razzaque, S., & Dermer, C. D. 2010, *ApJ*, 712, 238
- 720 Franceschini, A., Rodighiero, G., & Vaccari, M. 2008, *A&A*, 487, 837 (F08)
- 721 Georganopoulos, M., Sambruna, R. M., Kazanas, D., Cillis, A. N., Cheung, C. C., Perlman,  
722 E. S., Blundell, K. M., & Davis, D. S. 2008, *ApJ*, 686, L5
- 723 Greiner, J. et al. 2009, *A&A*, 598, 89
- 724 Gilmore, R. C., Madau, P., Primack, J. R., Somerville, R. S., & Haardt, F. 2009, *MNRAS*,  
725 399, 1694
- 726 Gould, R. J. & Shröder, G. 1966, *Phys. Rev. Lett.* 16, 252
- 727 Hauser, M. G., & Dwek, E. 2001, *ARA&A*, 39, 249
- 728 Healey, S. E., Romani, R. W., Taylor, G. B., Sadler, E. M., Ricci, R., Murphy, T., Ulvestad,  
729 J. S., & Winn, J. N. 2007, *ApJS*, 171, 61
- 730 Healey, S. E., et al. 2008, *ApJS*, 175, 97
- 731 Hopkins, A. M. & Beacom, J. F., 2006, *ApJ*, 651, 142
- 732 Katarzyński, K., Ghisellini, G., Tavecchio, F., Gracia, J., & Maraschi, L. 2006, *MNRAS*,  
733 368, L52
- 734 Kneiske, T. M., Mannheim, K. & Hartmann, D. H. 2002, *A&A* 386, 1
- 735 Kneiske, T. M., Bretz, T., Mannheim, K. & Hartmann, D. H. 2004, *A&A* 413, 807
- 736 Krennrich, F., Dwek, E., & Imran, A. 2008, *ApJ*, 689, L93
- 737 Madau, P., & Pozzetti, L. 2000, *MNRAS*, 312, L9
- 738 Malkan, M. A. & Stecker, F. W. 1998, *ApJ*, 496, 13
- 739 Malkan, M. A. & Stecker, F. W. 2001, *ApJ*, 555, 641

- 740 Marcha, M. J. M., Brown, I. W. A., Impey C. D., & Smith P. S. 1996, MNRAS,281, 425
- 741 Marconi, A. et al., 2004, MNRAS, 351, 169
- 742 Massaro, E., Giommi, P., Leto, C., Marchegiani, P., Maselli, A., Perri, M., Piranomonte,  
743 S., & Sclavi, S. 2009, A&A, 495, 691
- 744 Massaro, E., Tramacere, A., Perri, M., Giommi, P., & Tosti, G. 2006, A&A, 448, 861
- 745 Mattox, J. R., et al. 1996, ApJ, 461, 396
- 746 Mattox, J. R., Hartman, R. C., & Reimer, O. 2001, ApJS, 135, 155
- 747 Mazin, D. & Raue, M. 2007, A&A 471, 439
- 748 Mirizzi, A., Raffelt, G.G. & Serpico, P.D. 2007, Phys. Rev. D76, 023001
- 749 Murase, K., Takahashi, K., Inoue, S., Ichiki, K., & Nagataki, S. 2008, ApJ, 686, L67
- 750 Neronov, A., & Vovk, I. 2010, Science, 328, 73
- 751 Nishikov, A. I. 1961, Zh. Experimen. i Theo. Fiz. 41, 549
- 752 Plaga, R. 1995, Nature, 374, 430
- 753 Prandini, E., Bonnoli, G., Maraschi, L., Mariotti, M., & Tavecchio, F. 2010, MNRAS, L65
- 754 Primack, J. R., Bullock, J. S., & Somerville, R. S. 2005, in AIP Conf. Ser. 745, High Energy  
755 Gamma-Ray Astronomy, ed. F. A. Aharonian, H. J. Völk, & D. Horns (Melville, NY:  
756 AIP), 23
- 757 Protassov, R., van Dyk, D. A., Connors, A., Kashyap, V. L., & Siemiginowska, A. 2002,  
758 ApJ, 571, 545
- 759 Razzaque, S., Dermer, C. D., & Finke, J. D. 2009, ApJ, 697, 483
- 760 Razzaque, S., Mészáros, P., & Zhang, B. 2004, ApJ, 613, 1072
- 761 Reimer, A. 2007, ApJ, 665, 1023
- 762 Salamon, M. H., & Stecker, F. W. 1998, ApJ, 493, 547
- 763 Salvaterra, R., et al. 2009, Nature, 461, 1258
- 764 Sanchez-Conde, M. A., Paneque, D., Bloom, E. D., Prada, F., & Dominguez, A. 2009, Proc.  
765 of the 1st *Fermi* Symposium, eConf Proceedings C091122

- 766 Schroedter, M. 2005, *ApJ*, 628, 617
- 767 Serpico, P.D. 2009, *Adv. in Space Sci.* 43, 335
- 768 Sowards-Emmerd, D., Romani, R.W., & Michelson, P.F., 2003, *ApJ*, 590, 109
- 769 Stanev, T. & Franceschini, A. 1998, *ApJ*, 494, L159
- 770 Stecker, F. W., Baring, M. G., & Summerlin, E. J. 2007, *ApJ*, 667, L29
- 771 Stecker, F. W., Malkan, M. A. & Scully, S. T. 2006, *ApJ*, 648, 774 (St06), and Erratum:  
772 *ApJ*, 658, 1392 (2007)
- 773 Stecker, F. W., & de Jager, O. C. 1993, *ApJ*, 415, L71
- 774 Stocke, J. T., Morris, S. L., Gioia, I. M., et al. 1991, *ApJS*, 374, 72
- 775 Takahashi, K., Murase, K., Ichiki, K., Inoue, S., & Nagataki, S. 2008, *ApJ*, 687, L5
- 776 Tanvir, N. R., et al. 2009, *Nature*, 461, 1254
- 777 Tavani, M., et al. 2008, *Nucl. Instrum. Methods Phys. Res. A*, 588, 52
- 778 Thompson, D. J., et al. 1993, *ApJS*, 86, 629
- 779 Wagner, S.J. et al., (HESS Collaboration), 2010, 11th HEAD, BAAS, 42.
- 780 Wilks, S.S. 1938, *Ann. Math. Stat.*, 9, 60

Source	$z$	$E_{max}$	$\tau_{UL}(z, E_{max})$
J1147-3812	1.05	73.7	1.33
J1504+1029	1.84	48.9	1.82
J0808-0751	1.84	46.8	2.03
J1016+0513	1.71	43.3	0.83
J0229-3643	2.11	31.9	0.97
J1012+2439	1.81	27.6	2.41

Table 6: Opacity upper limits (95% c.l.) for AGN in Table 3. The first and second column report the name of the sources and their redshift, the third column the maximum photon energy and the fourth column the opacity UL evaluated at 95% c.l. as  $\tau_{UL} = \ln[F_{unabs}(E)/F_{obs}(E)] + 2\sigma$ .